AD-A015 090

WIDEBAND SOLID-STATE PHASED-ARRAY ANTENNA
DEVELOPMENT AT UHF

G. J. Laughlin

Johns Hopkins University

**PLEASE FOLD BACK IF NOT NEEDED
FOR BIBLIOGRAPHIC PURPOSES**

REPORT DOCUMENTATION PAGE

1. REPORT NUMBER	2. GOVT ACCESSION NO	3. RECIPIENT'S CATALOG NUMBER
APL/JHU TG 1278		

4. TITLE (and Subtitle)	5. TYPE OF REPORT & PERIOD COVERED
WIDEBAND SOLID-STATE PHASED-ARRAY ANTENNA DEVELOPMENT AT UHF	Technical Memorandum
	6. PERFORMING ORG. REPORT NUMBER

7. AUTHOR(s)	8. CONTRACT OR GRANT NUMBER(s)
G. J. Laughlin	N00017-72-C-4401

9. PERFORMING ORGANIZATION NAME & ADDRESS	10. PROGRAM ELEMENT, PROJECT, TASK AREA & WORK UNIT NUMBERS
The Johns Hopkins University Applied Physics Laboratory 8621 Georgia Avenue Silver Spring, Maryland 20910	

11. CONTROLLING OFFICE NAME & ADDRESS	12. REPORT DATE
Naval Plant Representative Office 8621 Georgia Avenue Silver Spring, Maryland 20910	July 1975
	13. NUMBER OF PAGES
	101

14. MONITORING AGENCY NAME & ADDRESS	15. SECURITY CLASS. (of this report)
Naval Plant Representative Office 8621 Georgia Avenue Silver Spring, Maryland 20910	Unclassified
	15a. DECLASSIFICATION/DOWNGRADING SCHEDULE
	N/A

16. DISTRIBUTION STATEMENT (of this Report)

Approved for public release; distribution unlimited.

17. DISTRIBUTION STATEMENT (of the abstract entered in Block 20, if different from Report)

N/A

18. SUPPLEMENTARY NOTES

N/A

19. KEY WORDS (Continue on reverse side if necessary and identify by block number)

Array antennas	Solid-state phased arrays
Phased arrays	Integrated phased arrays
Wideband phased arrays	Baluns
Octave band phased arrays	

20. ABSTRACT (Continue on reverse side if necessary and identify by block number) Development of an experimental 16-element solid-state linear phased-array antenna that has an operating band from 0.6 to 0.95 GHz is described. Radiating elements in the antenna are novel strip radiators made using printed circuit techniques. The array aperture has been impedance matched to a VSWR < 3.0:1 over the octave band from 0.5 to 1.0 GHz with beam scanning to ±60° in the H plane. Element patterns measured on a 10- by 10-element array aperture indicate that the aperture is also matched with beam scanning to ±60° in the E plane. Each of the radiators in the 16-element linear array was integrated with a microwave transistor amplifier with a nominal gain of 10 dB and efficiency of 50% at 3 watts output. Bandwidths of the amplifiers limit the 16-element solid-state array to an operating band from 0.6 to 0.95 GHz. Beam scanning in the H plane is accomplished by inserting lengths of coaxial delay lines between the integrated array and a 16:1 power divider network. Techniques and methods used in this development are applicable at higher radar frequencies.

DD FORM 1 JAN 73 **1473**

-1-
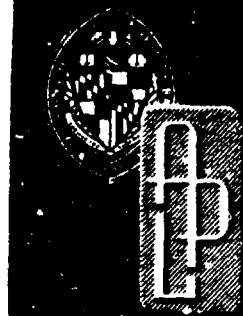
APL/JHU
TG 1278
JULY 1975

Technical Memorandum

WIDEBAND SOLID-STATE PHASED-ARRAY ANTENNA DEVELOPMENT AT UHF

G. J. LAUGHLIN

2

279140

ADA015090

Technical Memorandum

WIDEBAND SOLID-STATE PHASED-ARRAY ANTENNA DEVELOPMENT AT UHF

G. J. LAUGHLIN

D D C

SEP 29 1975

B

THE JOHNS HOPKINS UNIVERSITY ■ APPLIED PHYSICS LABORATORY

CONTENTS

ILLUSTRATIONS

1. INTRODUCTION

WIDEBAND SOLID-STATE PHASED-ARRAY ANTENNAS

Wideband phased-array antennas have been viewed as a solution to the proliferation of shipborne antenna systems resulting from the many and varied needs on naval vessels. The present large number of antennas could be consolidated into a single time-shared wideband aperture with electronic beam scanning. In recent years, solid-state microwave technology has advanced to the stage where increased reliability and efficiency of solid-state devices can be used advantageously for RF power generation in modern phased arrays. Integrating wideband solid-state power devices with a wideband array aperture would result in a highly reliable system with increased efficiency between DC power generation and RF transmission, reduce the number of shipborne antennas, and provide enhanced operational capabilities in an unfriendly environment. Also the wideband antenna capabilities have clear potential for countermeasure applications, both passive and active.

A wideband solid-state phased-array antenna with wide angle scanning was developed to demonstrate the feasibility of such a system for eventual shipborne application. An experimental very wideband system with beam scanning to $\pm 60^\circ$ was built for operation at UHF frequencies. This effort included investigations of techniques required to design an octave band (0.5 to 1.0 GHz) array aperture and methods for the efficient wideband generation of RF power. Designs used in this system were to be adaptable to higher radar frequencies.

APPROACH

Radiated power from a solid-state antenna aperture can be increased if the solid-state devices are integrated with electrically small radiating elements. The elements

- 9 -

Preceding page blank

can be closely spaced in the array aperture to combine effi-
ciently in free space the RF energy from many low-power
elements. In addition, the closely spaced elements help to
ease impedance matching of the antenna aperture over large
scan angles (Ref. 1). The Applied Physics Laboratory (APL)
has developed a strip radiator that is electrically small and
compatible with printed circuitry (Ref. 2). It appeared that
this radiator could be made with very wideband capabilities.
Therefore, we decided to develop an active band aperture
of these strip radiators closely spaced with beam scanning
to ±60°. The effort included modeling the element, gen-
erating design curves, fabricating an aperture for measure-
ment in a waveguide simulator, and constructing a 10- by
10-element aperture to measure element radiation patterns.

The solid-state device selected for RF amplification
in the array antenna is the microwave bipolar tran-
sistor with its inherent wide bandwidth. While there are a
number of solid-state devices capable of higher peak powers
and operation at higher frequencies, all are characterized
by relatively low DC-RF efficiency with resultant low aver-
age power and are generally restricted to narrowband sys-
tems. Microwave transistors have efficiencies as high as
70% and typically exhibit efficiencies of about 30% through
S-band, with average power in the several watt range. For
the solid-state array system, transistor amplifiers operat-
ing in the high efficiency class C mode were designed with
the objective of providing as wide a bandwidth as practical.

Lastly, a linear array of the active band elements
was integrated with the wideband amplifiers to form a solid-
state array. Array performance was measured in an an-
echoic chamber at the APL Antenna and Boresight Facility.

Ref. 1.   J. L. Allen, "On Array Element Impedance
Variation With Spacing," IEEE Transactions on Antennas
and Propagation, Vol. AP-12, May 1964, pp. 371-372.

Ref. 2.   E. V. Byron, "A New Flush Mounted An-
tenna Element for Phased Array Application," Proceed-
ings of the Phased-Array Antenna Symposium, 1970, pp.
187-192.

2. OCTAVE BAND ARRAY APERTURE

STRIP RADIATOR

Development of the octave band antenna is based on a phased-array radiating element, the strip radiator, that was developed for Project Camel (Refs. 2 and 3). Attractive features of the element are that it is configured using printed circuit techniques, it is suitable for integration with solid-state devices, and it can be densely packed in an array aperture.

Figure 1 shows an aperture of the strip radiators that was developed for Project Camel. It consisted of an array of conducting strips situated above a ground plane where a suitable dielectric filled the region between ground plane and strips. The strips were nominally a half wavelength wide in the dielectric and were excited periodically near the edges by probes extending through the ground plane. On each strip, probes were placed opposite one another and near the edge. The two probes at opposite edges were driven in antiphase with equal amplitudes. That development resulted in array apertures with half wavelength element spacing and bandwidths on the order of 10 to 12%. For Project Camel, the emphasis was on antennas with elements spaced very close to the ground plane.

In the present work, we felt both that a very wideband antenna aperture could be achieved by increasing the spacing between strips and ground plane and that close element spacing could be easily obtained in the H-plane by moving adjacent pairs of feed probes close together. Originally it was thought that close E-plane spacing could be achieved by dielectric loading to make the strips narrow ($\lambda/2$ in the dielectric), but, as the discussion of the strip radiator model in the next subsection shows, narrow strips and close E-plane spacing can be accomplished even without dielectric loading. The need for a compact and wideband antiphase power divider for driving the elements was

Ref. 3. E. V. Byron, Antenna Aperture Design for Project Camel, APL/JHU TG 1101, February 1970.

- 11 -
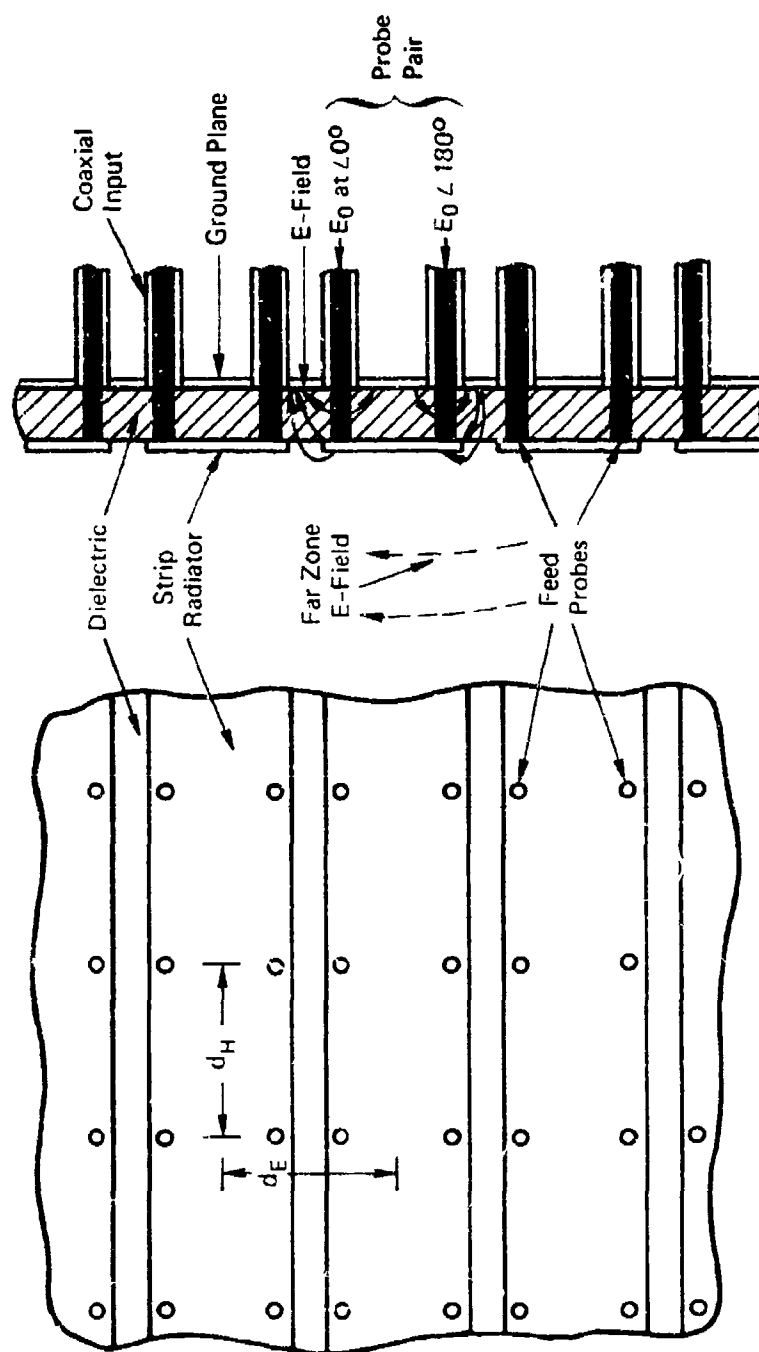
Fig. 1 Array of Strip Radiators

recognized. this required an additional development effort which is discussed in the subsection on the antiphase feed network.

Aperture resonance, which can be initiated by dielectric impedance matching sheets on an array aperture, was the limiting factor in an earlier wideband antenna design (Ref. 4). To avoid these resonances as much as possible with the strip radiators, where dielectric loading is inherent in the design, the aperture impedance matching was implemented in this design by networks behind the aperture rather than by additional dielectric sheets.

STRIP RADIATOR MODEL

A large planar phased-array aperture can be simulated with relatively few elements in waveguide to determine aperture radiation performance (Ref. 5). A waveguide excited in the TE_{10} mode may be considered to contain two inclined plane waves propagating down the guide. The angle each of the plane waves makes with the longitudinal direction (Fig. 2) is determined by the H-dimension of the waveguide and simulates the angle of scan of an infinite array:

$$\sin \theta = \lambda/\lambda_c . \qquad (1)$$

Additional scan angles may be simulated by exciting other modes. The waveguide dimensions are chosen so that a radiating element (or elements) placed in the waveguide

Ref. 4.   G. J. Laughlin, E. V. Byron, and T. C. Cheston, "Very Wideband Phased-Array Antenna," IEEE Transactions on Antennas and Propagation, Vol. AP-20, November 1972, pp. 699-704.

Ref. 5.   P. W. Hannan and M. A. Balfour, "Simulation of a Phased-Array Antenna in Waveguide," IEEE Transactions on Antennas and Propagation, Vol. AP-13, May 1965, pp. 342-353.
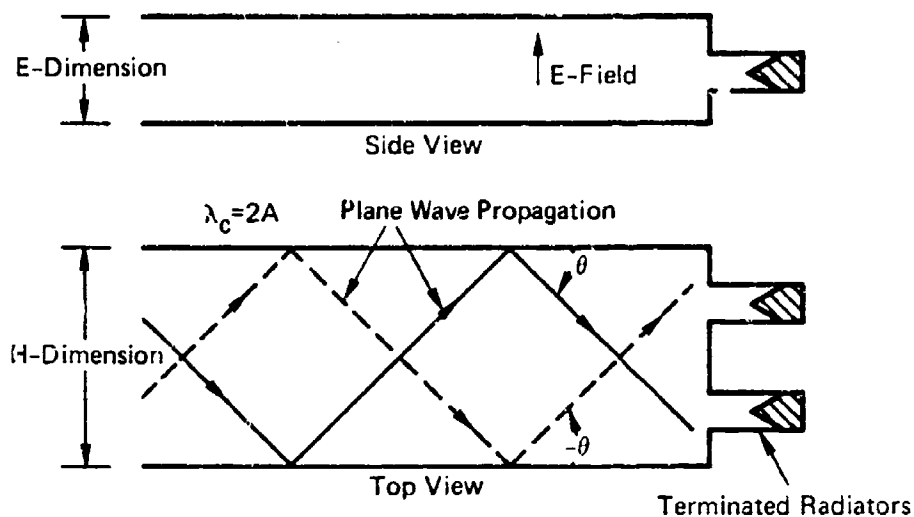
Fig. 2 Array Simulator Terminated in Two Elements

sees mirror images in the walls of the guide that appear
to be at the same spacing as the array to be simulated.
Excitation of the waveguide in the TE_{10} mode simulates
H-plane scanned conditions on the infinite array.

A model for an array of strip radiators can be de-
veloped that is based on the array aperture simulated in
waveguide. The aperture equivalent circuit under H-plane
scanning conditions is derived from the equivalent circuits
for obstacles in waveguide. Let us consider an array of
the strip radiators with rectangular element spacing simu-
lated in waveguide as depicted in Fig. 3. The height of the
waveguide is one-half the E-plane spacing so that only a
single feed probe of each radiator is included. The model
is presented to show the air-filled simulator (i.e., the re-
gion to the left of the radiator strip in the figure) and the
aperture dielectric region as separate waveguide sections
coupled by a slit. In the aperture dielectric region an
array of probes excites an electric field between strip and

- 14 -
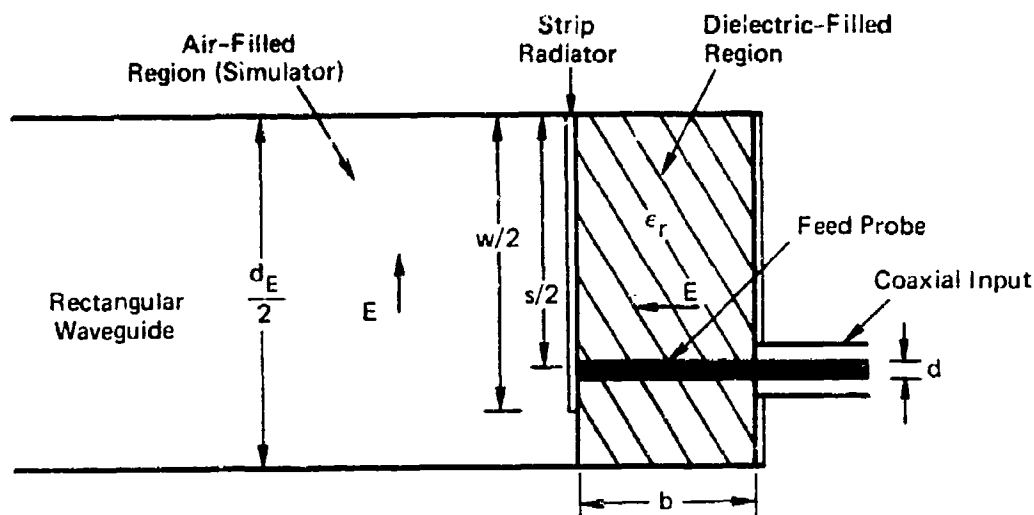
Fig. 3 Strip Radiator in Waveguide Simulator

ground plane (horizontal polarization in the figure), and a
short circuited length of guide is paralleled across the
probes. These waveguide obstacles are considered sepa-
rately in arriving at the array aperture equivalent circuit.
Implicit in this model is the assumption that coupling slit,
probes, and short circuit are sufficiently separated that
coupling through fringing fields between obstacles is negli-
gible.

Detailed derivations of the waveguide obstacles and
of the aperture equivalent circuit are given in Appendix A.
Figure 4, reproduced from Appendix A, shows the result-
ing array aperture equivalent circuit. Summarizing the
appendix, this circuit considers the antenna impedances
on a half-unit cell basis where one feed probe is included
in each half-cell. The resistance, R_p, is the probe coax-
ial termination. The free space impedance, Z_{fs} is shown
in Appendix A (Eq. (A-12)) to be
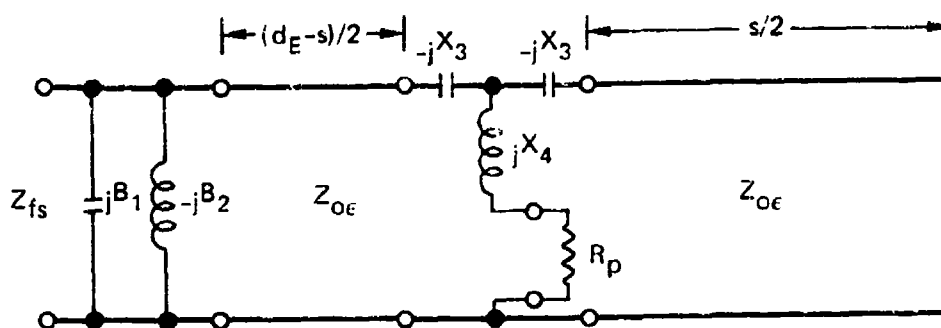
Fig. 4 Equivalent Circuit, Array of Strip Radiators (H-plane scan)

$$Z_{fs} = \frac{1}{2} (d_E/d_H) \, x/\cos \theta_o \, .$$

Equations (A-17) through (A-23) give the remaining imped-
ance elements in the equivalent circuit.

STRIP RADIATOR DESIGN PROCEDURE

The method for designing an array of printed cir-
cuit radiators with given E- and H-plane spacings considers
the center frequency broadside active element impedance of
a half-element as seen at the feed probe inputs. The feed
probes are assumed to be purely inductive in this proce-
dure (i.e., in Fig. 4 $X_3 = 0$). Element parameters are
chosen to make the resistive part of the active element im-
pedance (of a half-element) equal to the coaxial termination
(generator) impedance at each probe, typically 50 ohms.
The antenna reactance is cancelled by selecting the probe
dimensions and, if necessary, inserting a capacitor in
series with the probe. In the case of ribbon probes, the

- 16 -

best capacitor location has been found experimentally to be
midway between strips and ground plane.

The first step in the design is to plot the re-
sistive part, R(w), of the active element impedance for
the feed probes located at the strip edges. Curves of R(w)
versus w/d_E for the specific examples of square spacing
with $d_E/\lambda = 0.5$ and 0.238 and for several values of dielec-
tric constant, ϵ_r, are given in Figs. 5 through 10.

Secondly, the effects of moving the probes inward
from the strip edges are determined. An analysis of the
effects on the resistive part of the broadside active ele-
ment impedance, given in Appendix B, results in Eq. (B-5):

$$\frac{R(s)}{R(w)} \approx \left(1 - \frac{(1 - s/w)\, \beta_\epsilon\, w/2}{\tan (\beta_\epsilon\, w/2)}\right)^2$$

This equation is plotted in Fig. 11. The resistance change
with probe location is used to adjust the resistance, R(s), to
match the coaxial termination.

Summarizing, the design procedure is to select a
convenient set of values for aperture dielectric, thickness,
and strip width using Figs. 5 through 10. The probe sepa-
ration is picked using Fig. 11 to adjust R(s) to match the
probe termination (generator) impedance. For the selected
parameters the resulting reactance is cancelled by choosing
appropriate probe dimensions according to Eq. (A-20) from
Appendix A and, if necessary, incorporating a series capaci-
tor in each probe. It is then necessary to computer ana-
lyze the designed aperture to examine bandwidth and scan-
ning capabilities, using several iterations of designs from
the above procedure to meet specifications.

- 17 -
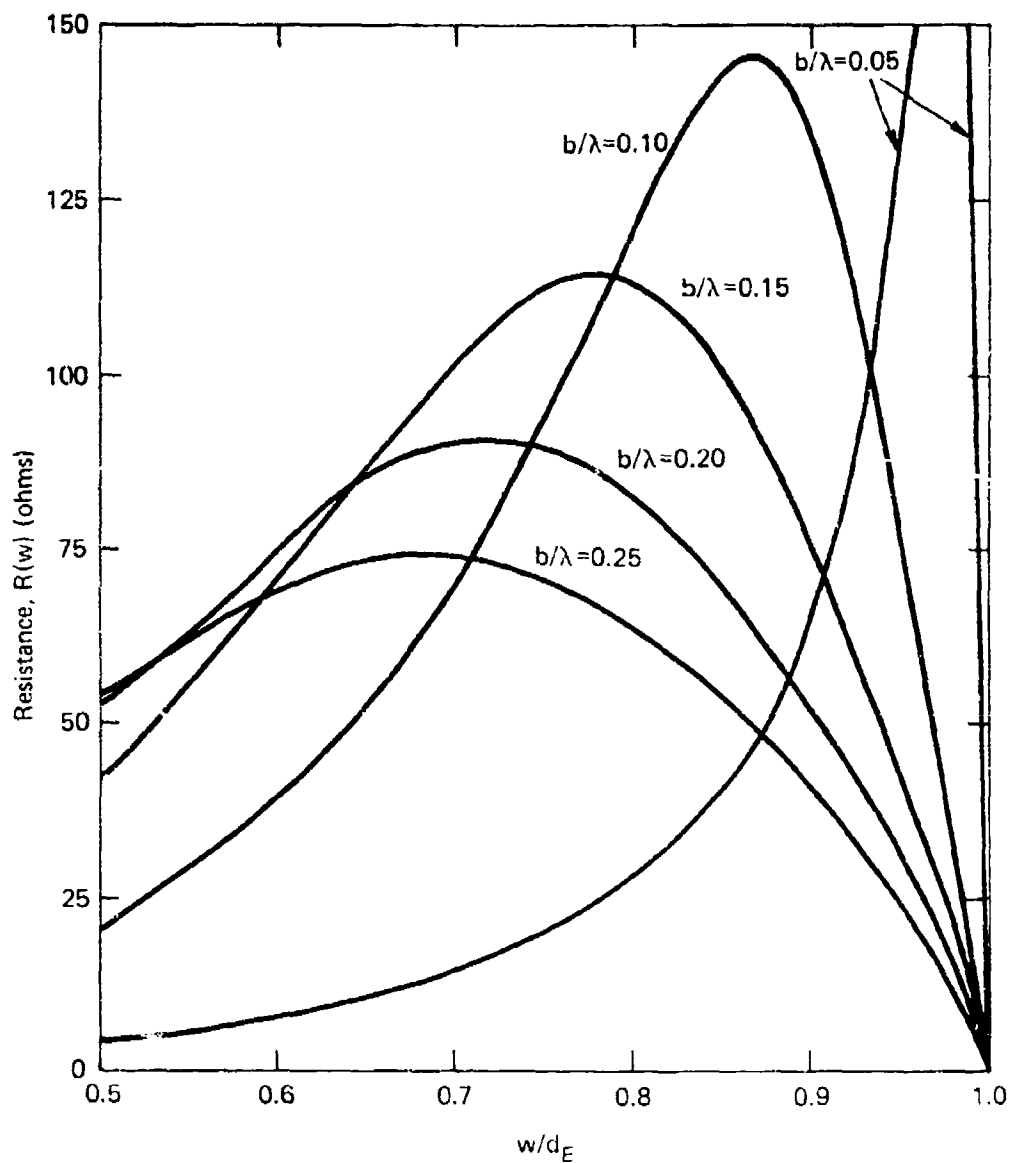
Fig. 5   Resistive Part of Active Element Impedance (per feed probe) versus
w/d$_E$; ϵ_r=1, d$_E$/λ=d$_H$/λ=0.238
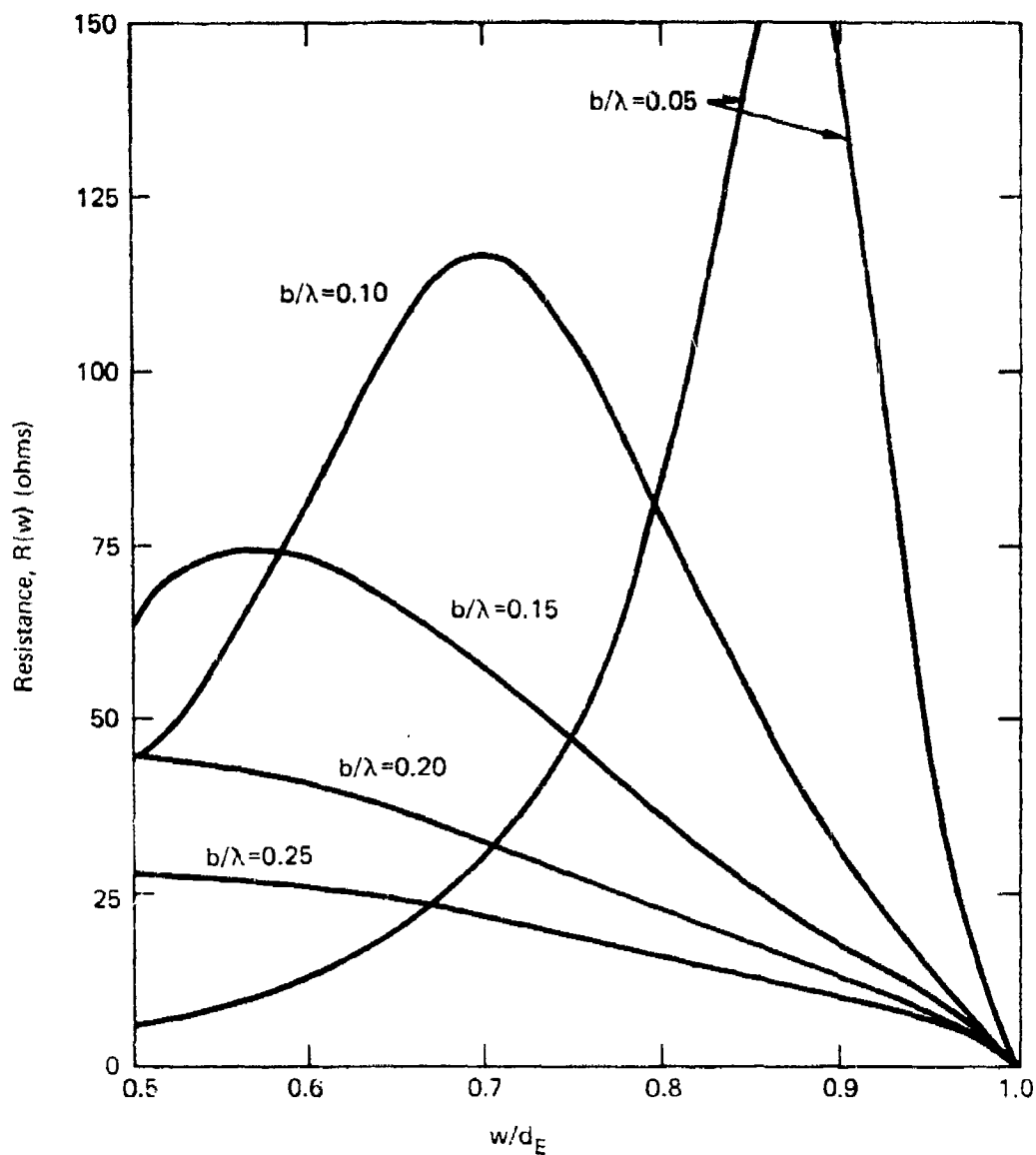
Fig. 6 Resistive Part of Active Element Impedance versus
w/d_E; ϵ_r=2.5, $d_E/\lambda=d_H/\lambda$=0.238

- 19 -
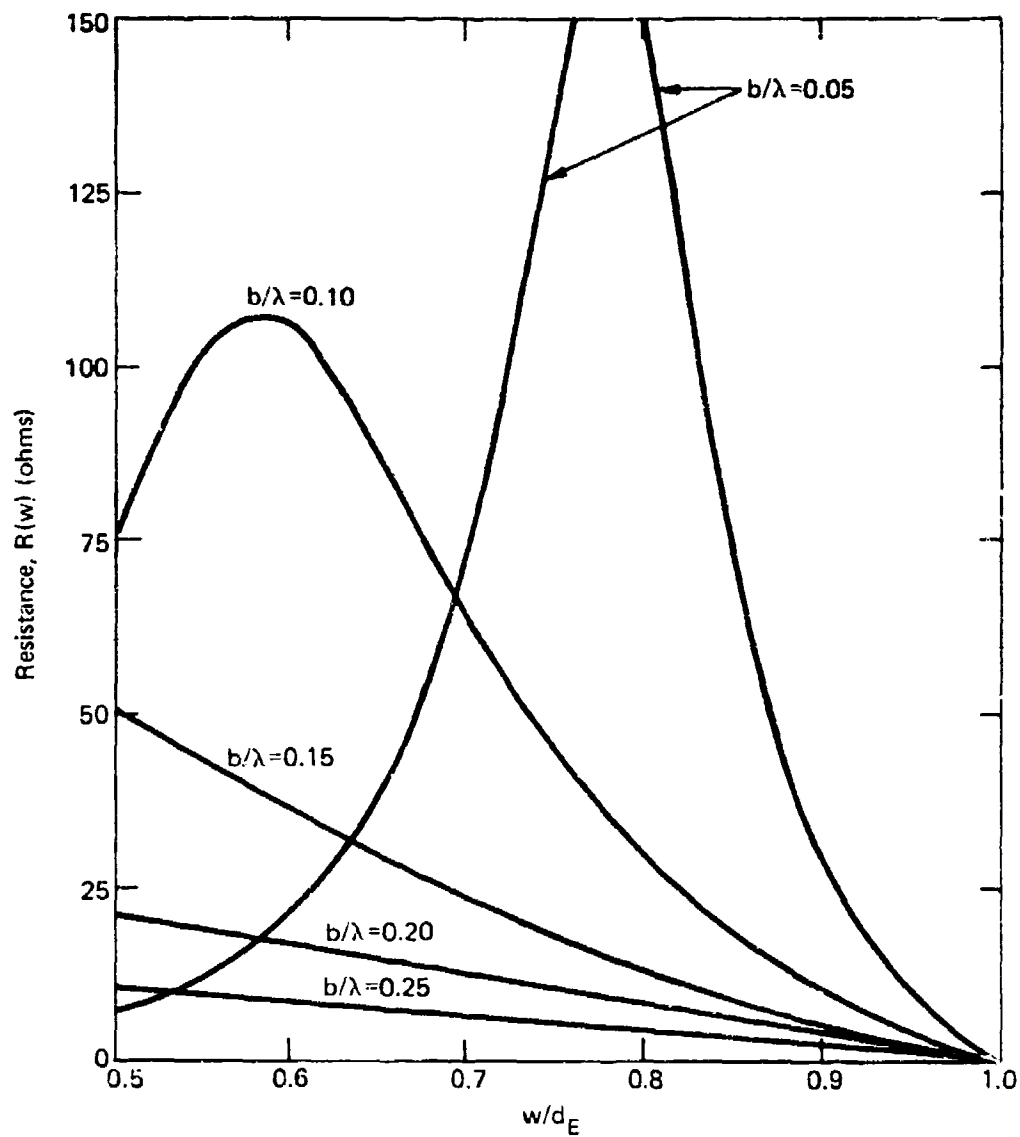
Fig. 7 Resistive Part of Active Element Impedance versus w/d_E; $\epsilon_r=4$, $d_E/\lambda=d_H/\lambda=0.238$
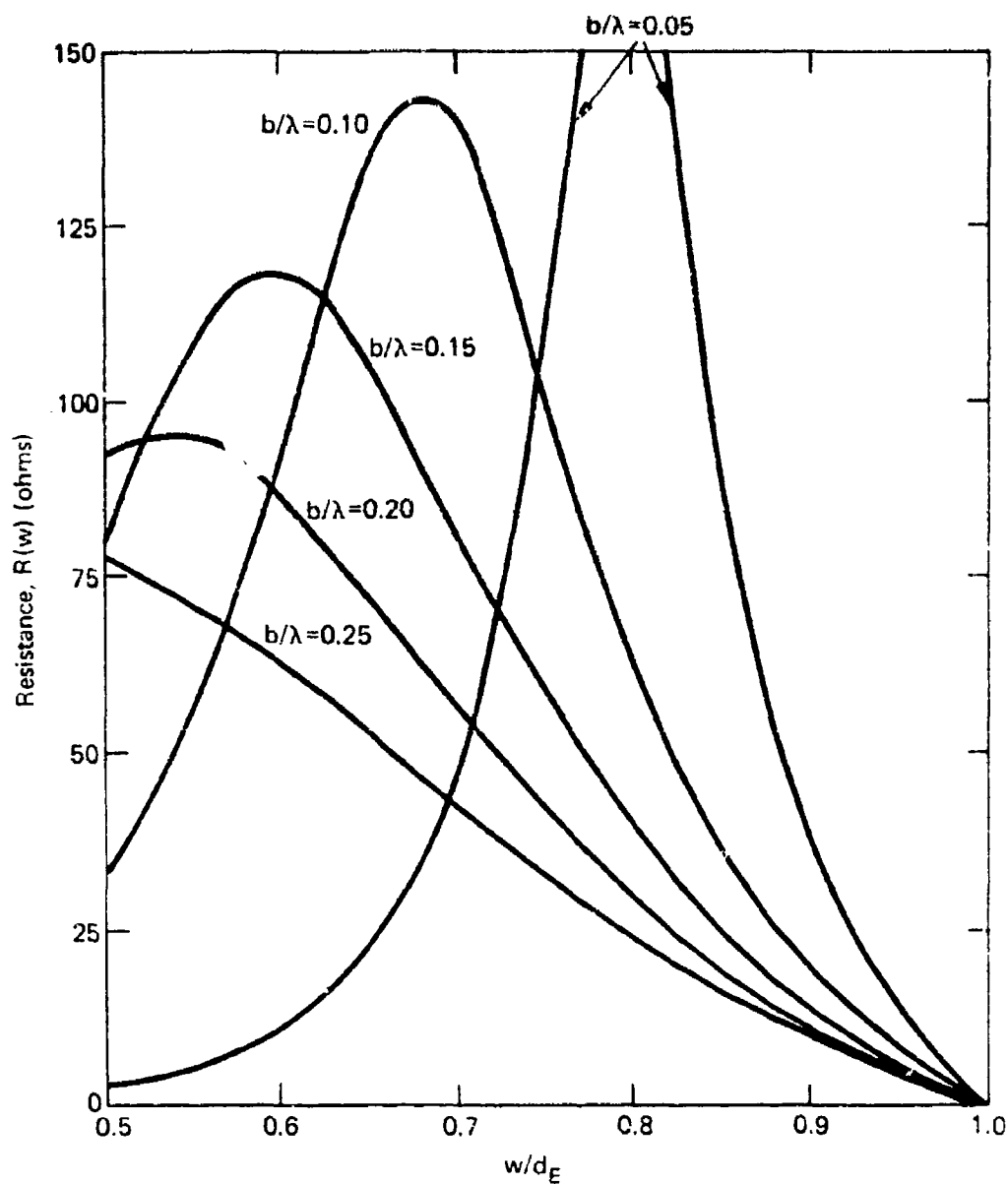
Fig. 8   Resistive Part of Active Element Impedance versus w/d_E; $\epsilon_r=1$, $d_E/\lambda=d_H/\lambda=0.5$
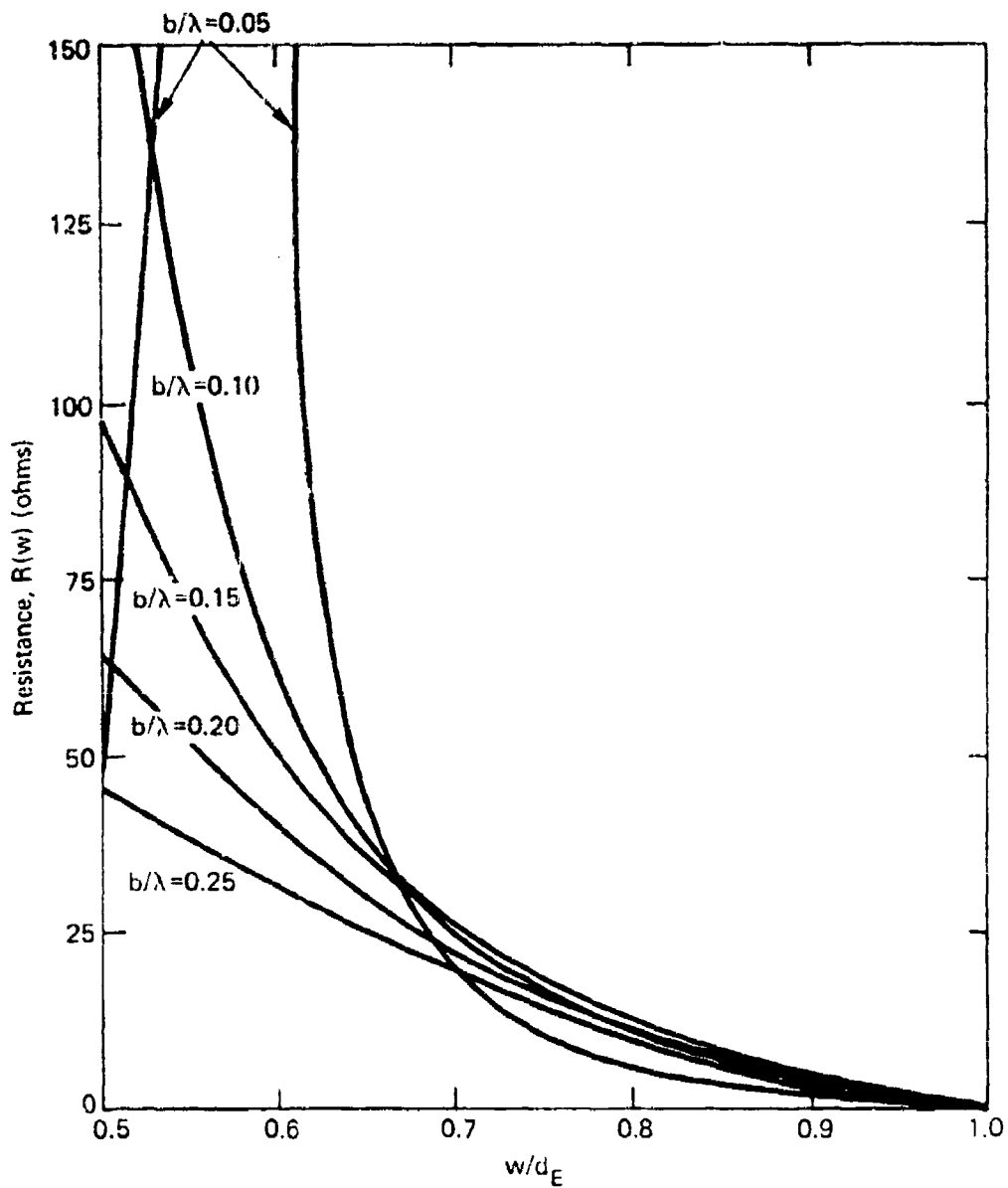
Fig. 9 Resistive Part of Active Element Impedance versus
w/d_E ; ϵ_r=2.5, d_E/λ=d_H/λ=0.5

- 22 -
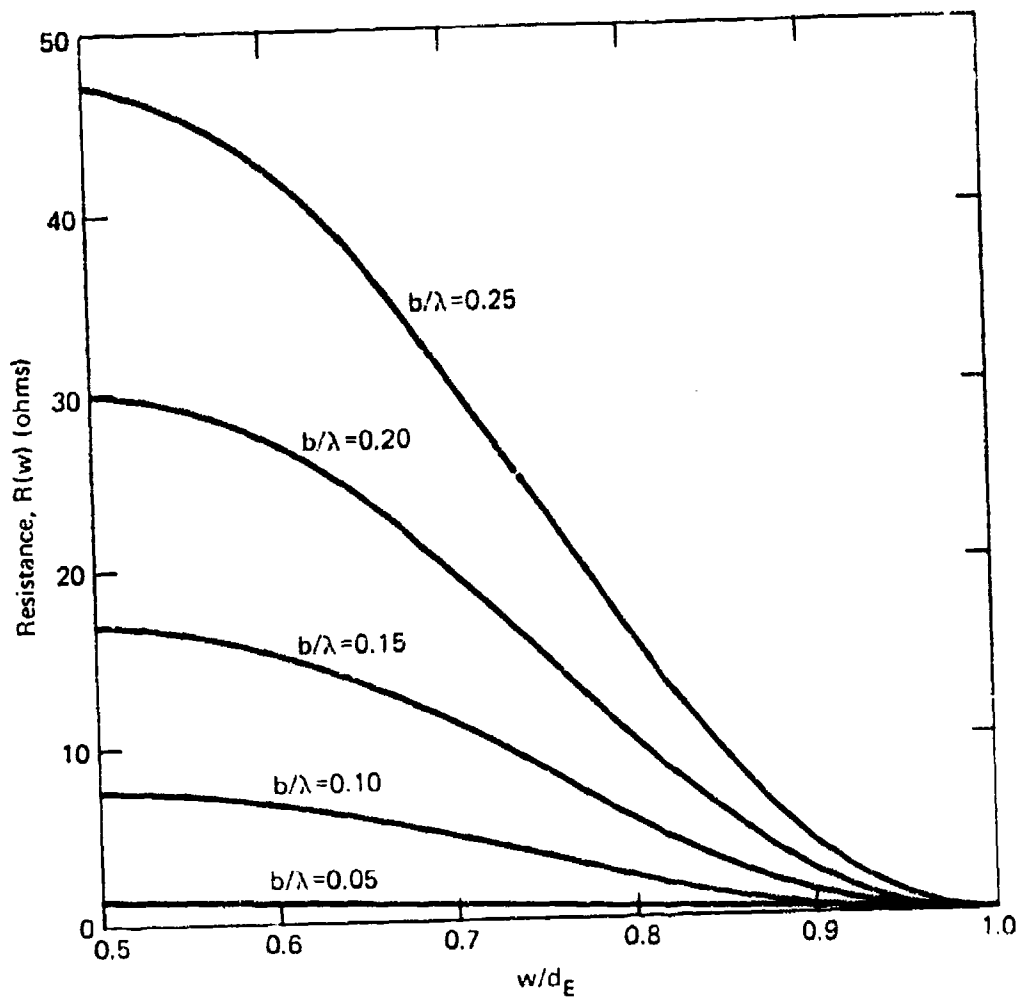
Fig. 10 Resistance Part of Active Element Impedance versus
w/d_E; $\epsilon_r=4$, $d_E/\lambda=d_H/\lambda=0.5$

- 23 -
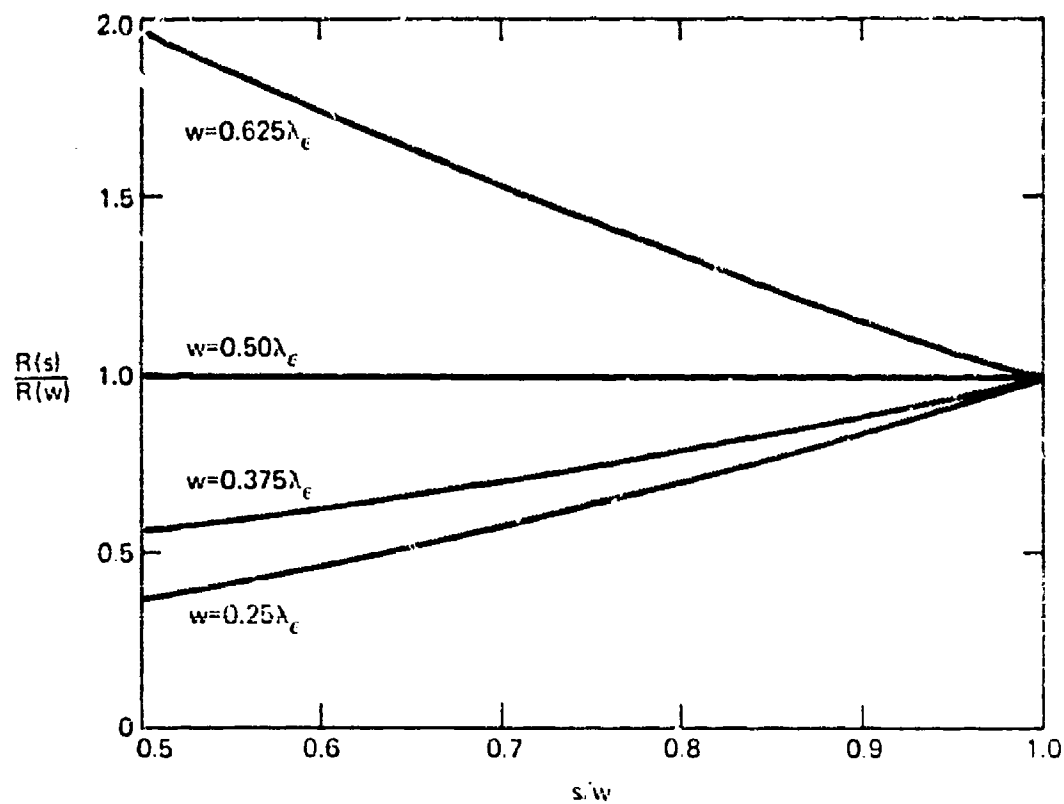
Fig. 11 Effects of Probe Separation on Resistive Part of Element Impedance

EQUAL AMPLITUDE ANTIPHASE FEED NETWORK

As discussed previously, the strip radiator requires the two feed probes to be driven in antiphase and equal amplitude over an octave bandwidth. It is desirable to achieve this by means of stripline circuitry. A device that can perform the antiphase and equal amplitude function is a modified balanced-to-unbalanced transmission line converter (the balun) in which the balanced line is in the form of a pair of antiphase unbalanced lines. Several authors have described baluns that operate over wide frequency ranges (Refs. 6 through 11). A series-connected balun developed for the strip radiator differs from the earlier devices by its method of achieving input-to-output coupling, resulting in an easily fabricated balun applicable to strip-line circuitry.

The coaxial circuit of the balun for the strip radiator is shown in Fig. 12 (from Ref. 12). The outer conduc-

Ref. 6.   N. Marchand, "Transmission-Line Conversion," Electronics, Vol. 17, December 1944, pp. 142-145.

Ref. 7.   W. K. Roberts, "A New Wideband Balun," Proceedings of the IRE, December 1957, pp. 1628-1632.

Ref. 8.   J. W. McLaughlin, D. A. Dunn, and R. W. Grow, "A Wideband Balun," IRE Transactions on Microwave Theory and T   ques, Vol. MTT-6, July 1958, pp. 314-316.

Ref. 9.   R. Bawer and J. J. Wolfe, "A Printed Circuit Balun for Use With Spiral Antennas," IRE Transactions on Microwave Theory and Techniques, Vol. MTT-8, May 1960, pp. 319-325.

Ref. 10.   G. Oltman, "The Compensated Balun," IEEE Transactions of Microwave Theory and Techniques, Vol. MTT-14, March 1966, pp. 112-119.

Ref. 11.   H. R. Phelan, "A Wideband Parallel-Connected Balun," IEEE Transactions of Microwave Theory and Techniques, Vol. MTT-18, May 1970, pp. 259-263.

Ref. 12.   G. L. Laughlin, Patent 3,827,001, July 1974.

- 25 -
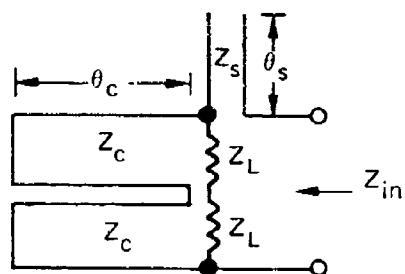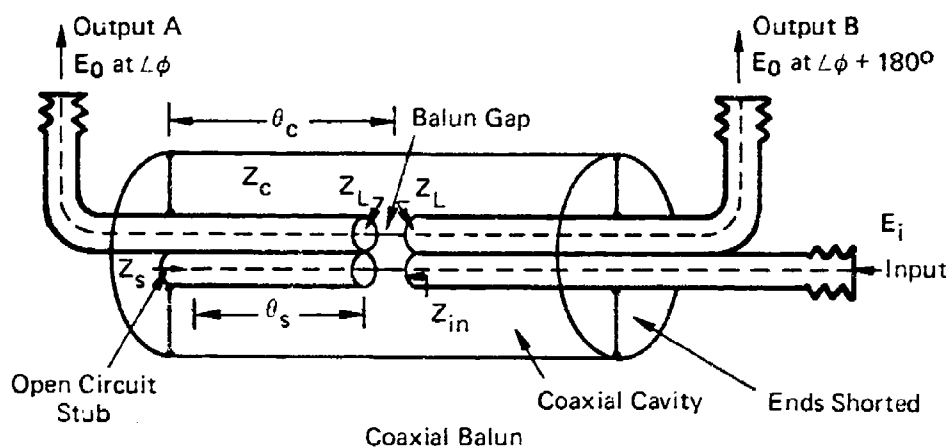
Fig. 12 Coaxial Series-Connected Balun

tors of adjacent coaxial lines are joined together. A cavity, nominally a half wavelength long, encloses the balun and is shorted to the coaxial lines at each end. A balanced parallel line output may be formed if the output lines are bent together outside the cavity and the center conductors extended forming a parallel transmission line. Coupling in the balun occurs at the gap formed by a break in the outer conductors of the coaxial lines across which an electric field is excited by an incident power flow in the input line. An electric field could also be excited if outputs A and B were driven in antiphase and equal amplitude. If a field is excited across the gap due to RF flow in a coaxial line, then, by reciprocity, an impressed electric field across the gap will induce power flow in the line. Thus, the field excited by the input coaxial lines couples RF powers into the output coaxial lines. For a small gap ($\approx \lambda/100$) the excited field is uniform, and the coupled powers are equal amplitude and in antiphase. Impedances of the outputs are series connected as shown in the equivalent circuit.

The enclosing cavity has the effect of paralleling a pair of series-connected short circuit stubs ($\lambda/4$ long) across the series-connected loads. Each of the short-circuit stubs is coaxial, with the outer conductor being the cavity and the center conductor being the shields of the enclosed coaxial lines. In Fig. 12, an open circuited stub, nominally a quarter wavelength long, is connected directly to the input line and appears in the equivalent circuit as a reactance in series at the input. The presence of the stub makes the balun "compensated." This stub can be replaced by a dummy solid rod that maintains gap symmetry and results in an "uncompensated" balun. The input impedance of the compensated balun as seen within the input line and referenced at the gap is

$$Z_{in} = \frac{Z_c Z_s \tan \theta_c \cot \theta_s + j Z_L (2 Z_c \tan \theta_c - Z_s \cot \theta_s)}{Z_L + j Z_c \tan \theta_c} . \quad (2)$$

A stripline modification of this balun was built for the octave band covering 0.5 to 1.0 GHz (Fig. 13). The input and output center conductors were of planar construction

- 27 -
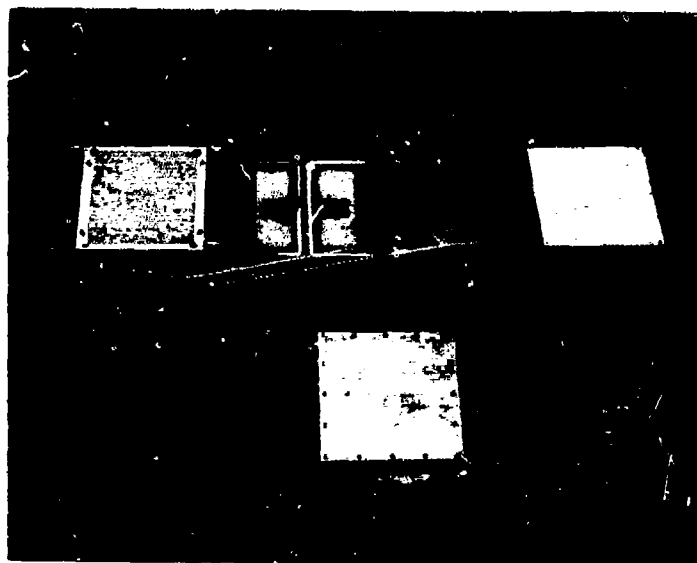
Fig. 13 Stripline Balun

on a stripline substrate (ϵ_r = 2.5, b = 0.167 inch). The outer
conductors were etched lines 1.27 inches wide such that
one pair of upper and lower lines enclosed the center con-
ductors, the pair being joined by eyelets. We eliminated
the shielding between input and output center conductors
(normally formed by eyelets) from the design by separat-
ing the conductors so that line coupling was less than 30 dB.
Balun coupling was through a 0.100-inch gap in the outer
conductor. The design, which was for 50-ohm input and
output impedances, was achieved by including a 35-ohm
quarter wavelength transformer in each output arm. The
output ports were spaced 2.75 inches apart to meet require-
ments of the strip radiator discussed in a following subsec-
tion. The balun cavity was formed by a dielectrically filled
(ϵr = 2.5) rectangular box 1.125 inches high giving a cavity
impedance of approximately 50 ohms. The total cavity
length was shortened to 0.28 λ at midband to accommodate
the required spacing at the output ports. Impedance match-
ing, required because of the shortened cavity, was done ex-
perimentally and resulted in placing a compensating 38-ohm

- 28 -

open circuit stub 0.13 inch wide and 0.18λ in length at mid-
band, and placing capacitive stubs, located at the gap, on
the coaxial outer conductor. Measured results of the feed
network are given in Fig. 14. The input VSWR over the
octave band is under 1.5:1, insertion loss is less than
0.4 dB, and maximum phase error is 2.6°.
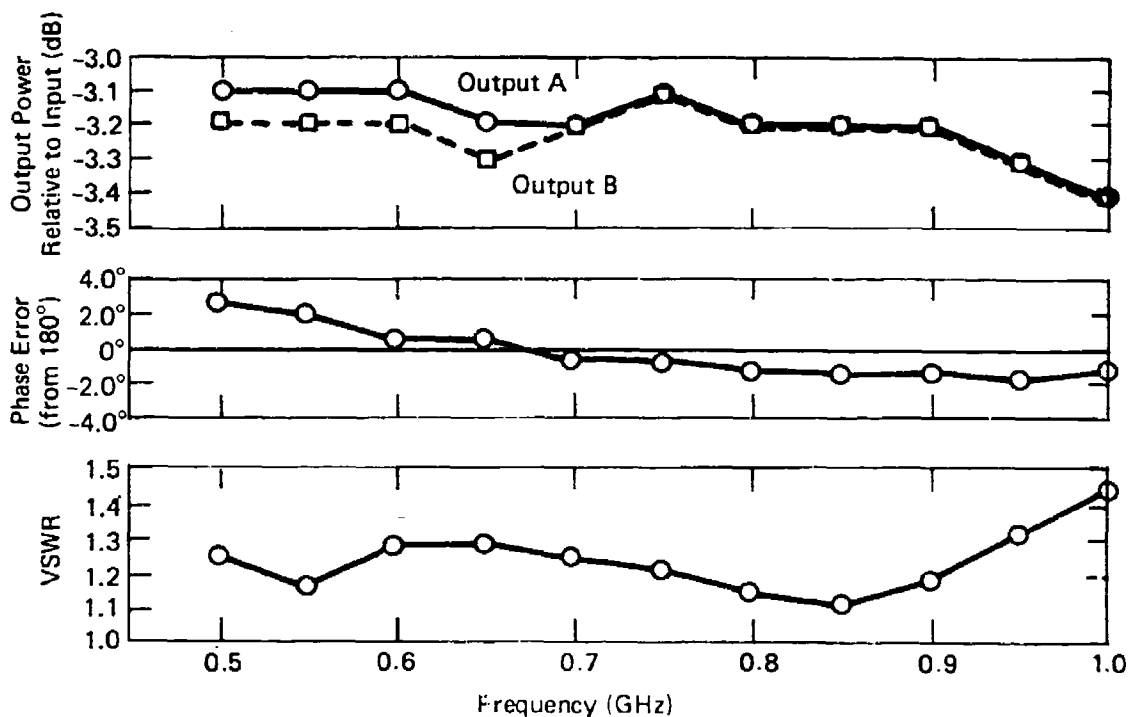
Fig. 14 Measured Results, Stripline Balun

For application with the strip radiator, we enlarged
the balun stripline substrate and extended the output center
conductors as shown in Fig. 15. The extended conductors
form the feed probes and are soldered to the radiating ele-
ment strip. A gap is etched in each probe to accommodate
a 2.2-pF capacitor included in the element design.

- 29 -
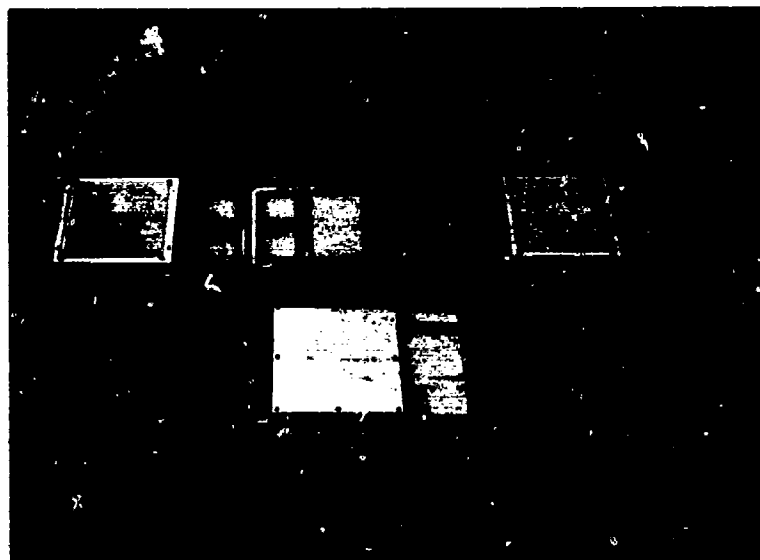
Fig. 15 Strip Radiator Feed Balun and Feed Probes

UHF APERTURE

An array aperture of the strip radiators was de-
signed for the octave band covering 0.5 to 1.0 GHz. The
antenna used square element geometry with close E- and
H-plane spacing of 3.75 inches (0.238 λ at midband). Aper-
ture excitation was by flat probes oriented such that each
pair of probes in an element was coplanar (perpendicular
to strip edges). The design was that each probe terminated
in 50 ohms.

Design parameters for the aperture, based on the
computer analysis of bandwidth and scanning performance,
were an aperture dielectric 1.5 inches thick with ϵ_r = 2.5,
a strip width of 3.1 inches, and probe separation of 2.75
inches. Referring to the design curves, we found that this
configuration yielded an active element impedance at mid-
band with a 57-ohm resistive part. The reactance, obtained
in the aperture analysis, was cancelled by making the probe
width 0.200 inch and incorporating a 2.2-pF capacitor in
series, located midway in the dielectric. Predicted per-

- 30 -

formance of the aperture was a VSWR under 3.5:1 over the octave band with scanning to ±45° in the H-plane. A listing of the computer program (Conversational Programming System language) and a printout for the above H-plane aperture impedances are given in Appendixes C and D, respectively.

An aperture for measurement in a waveguide simulator was constructed using polystyrene for the dielectric and copper foil tape for the strips. Eight strip radiators were included in the simulation. The probes were fabricated using stripline with the ground planes etched away in the aperture dielectric region. The coaxial lines extended behind the aperture ground plane and were terminated in 50 ohms. At the other end the extended center conductors were soldered to the strip.

When compared with the calculated data for the simulated angles, admittance measurements were more capacitive than predicted. We found that trimming the strip width to 3.0 inches gave closer correlation to the calculated values for a 3.1-inch strip (Fig. 16).

Octave band feed networks as described above, with a VSWR under 1.5:1 over the 0.5 to 1.0 GHz octave band, were built and incorporated in a simulated array. Figure 17 is a photograph showing the aperture and feed network. In this array a lightweight dielectric (Eccofoam Hik 625D) with $\epsilon_r = 2.5$ was used. Otherwise the aperture was the same as above. The feed networks used stripline construction, and the extended center conductors of the outputs formed the feed probes. Measured data on this aperture were nearly identical to those with each probe individually terminated in 50 ohms.

Simulated Aperture
d_E=3.75 inches
d_H=3.75 inches
Strip Width=3.0 inches
Probe Separation=2.75 inches
Probe Width=0.200 inch
ϵ_r=2.5, b=1.50 inches, 2.2 pF Capacitor

Predicted (for 3.1 inch Strip)

1.0 GHz
Measured
0.6 GHz
0.9 GHz   0.7 GHz
0.5 GHz   0.8 GHz
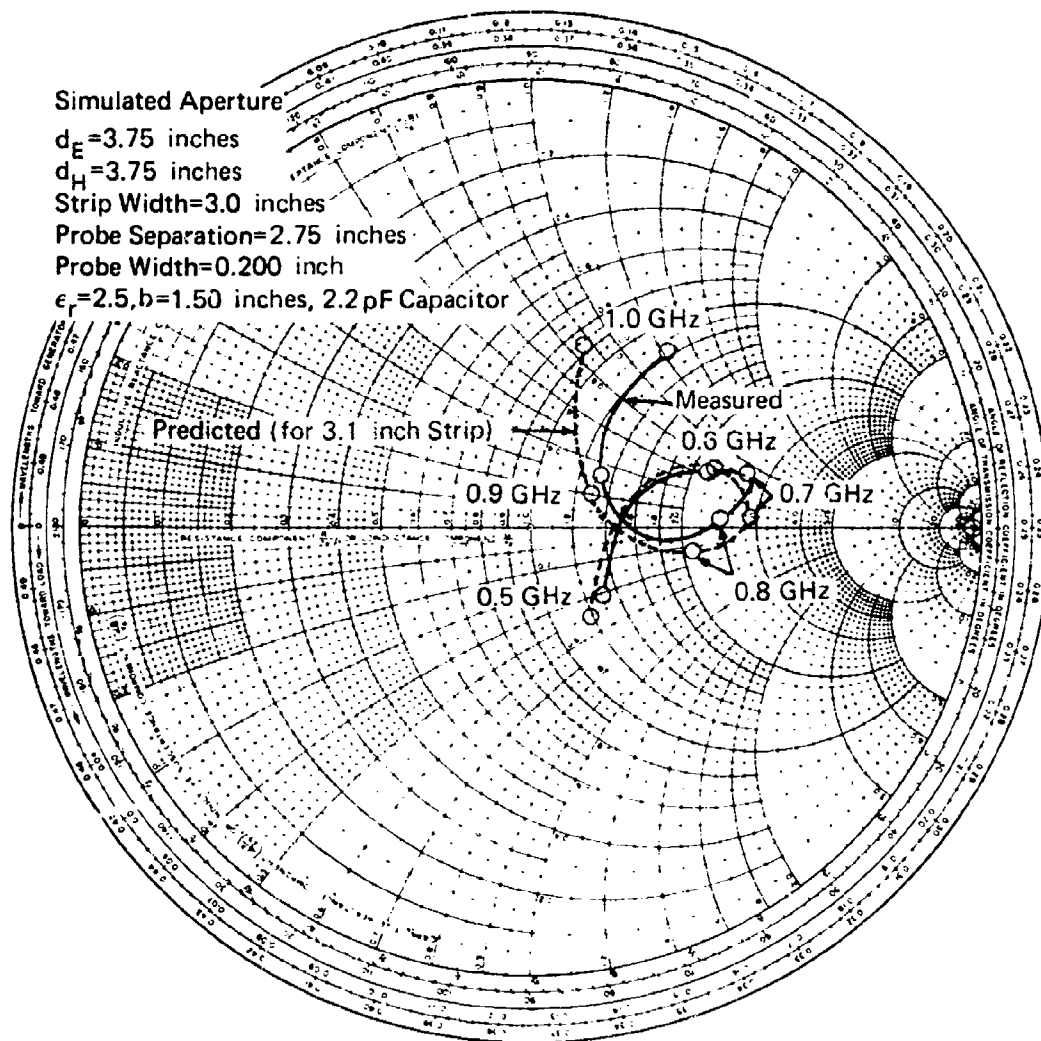
Fig. 16 Admittance of Simulated Array of Strip Radiators

- 32 -
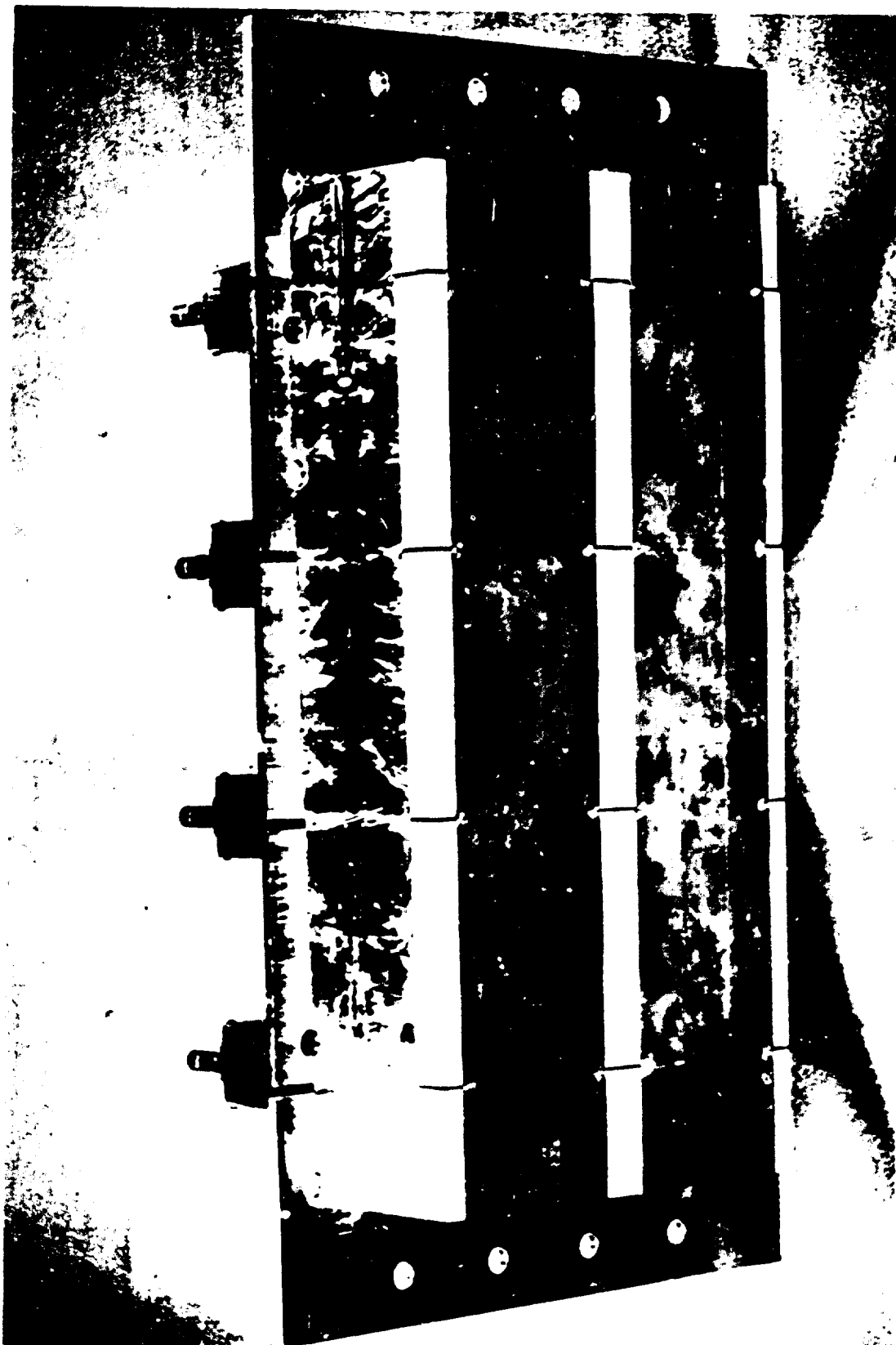
Fig. 17 Simulated Array Aperture of Printed Circuit Radiators

A final modification to the aperture was to use a wide-angle impedance matching (WAIM) technique developed by McGill and Wheeler (Ref. 13) to improve scanning performance. The technique uses a thin, planar, dielectric sheet with a high relative constant, that is as large as the aperture and is placed in front of and parallel to the array face. The admittance of the sheet is susceptive and is dependent on both scan angle and polarization. For a thin dielectric sheet the susceptance at broadside is given by

$$\frac{B(0)}{Y_o} = (\epsilon_r - 1)\frac{2\pi h}{\lambda}. \tag{3}$$

The susceptance variations with scan angle in the E- and H-planes are

$$\text{E-plane:} \quad \frac{B(\theta)}{B(0)} = \cos\theta - \frac{\sin^2\theta}{\epsilon_r \cos\theta}; \tag{4}$$

$$\text{H-plane:} \quad \frac{B(\theta)}{B(0)} = \frac{1}{\cos\theta}. \tag{5}$$

Referring to the Smith chart plot of calculated aperture admittance (for a 3.1-inch strip) given in Fig. 18, we can see that a 0.125-inch dielectric sheet with $\epsilon_r = 9$, spaced 2.00 inches in front of the aperture, can improve H-plane scan performance to a VSWR of less than 3.0:1 for scanning to 60° over the 0.5 to 1.0 GHz band. VSWR measurements with the WAIM on the aperture (trimmed to a 3.0-inch strip width) were performed in a waveguide simulator with the results shown in Fig. 19. The measured values correlate reasonably well with predicted values.

A 10- by 10-element array was constructed to measure element patterns and thus to verify H-plane performance and observe E-plane characteristics. An antiphase

Ref. 13. E. G. Magill and H. A. Wheeler, "Wide-Angle Impedance Matching of a Phased Array Antenna by a Dielectric Sheet," IEEE Transactions on Antennas and Propagation, Vol. AP-14, January 1966, pp. 49-53.
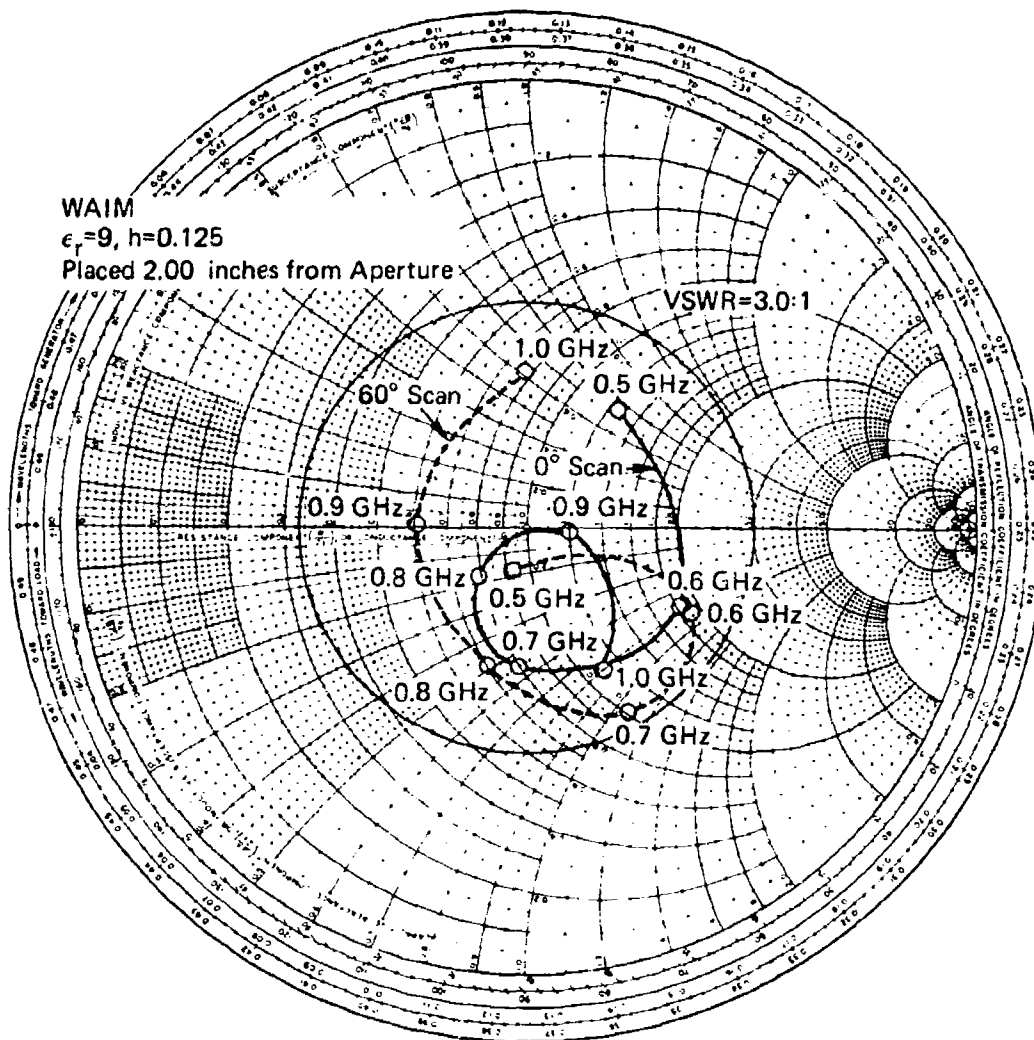
Fig. 18 Admittance with WAIM (predicted for 3.1-inch strip) Referenced at WAIM Sheet

- 35 -

WAIM: ϵ_r=9.0, h=0.125 inch Placed 2.00 inches in Front of Aperture
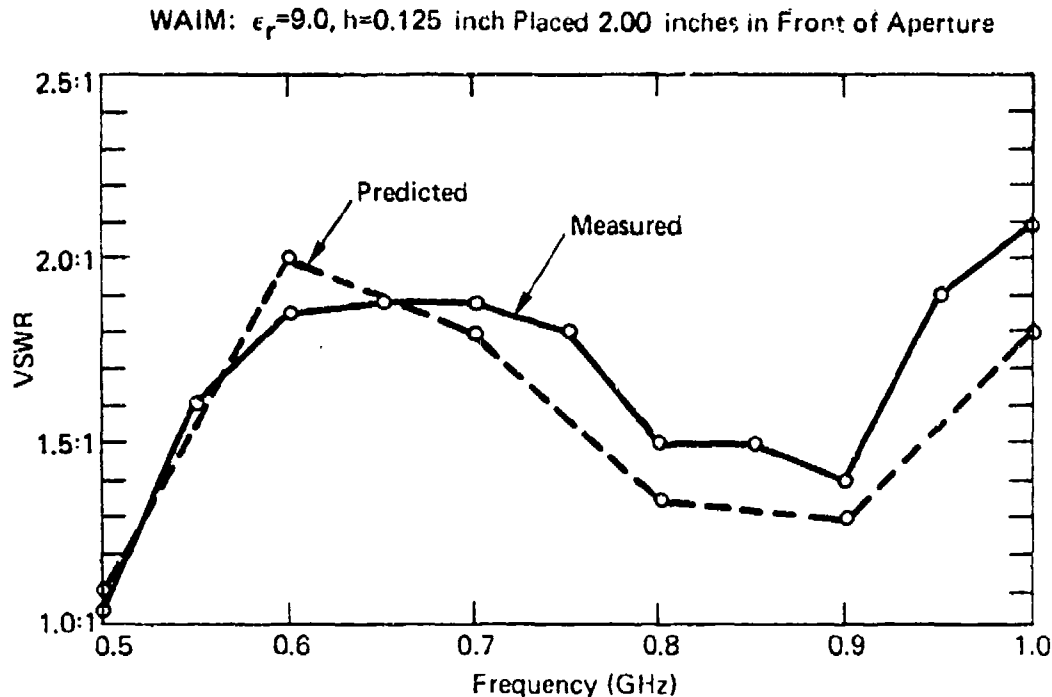
Fig. 19 VSWR of Simulated Array with WAIM

power divider was included for each element, and the divider input ports were individually terminated in 50 ohms. Measured element patterns in E- and H-planes with and without WAIM for frequencies of 0.5, 0.75, and 1.0 GHz are given in Figs. 20 through 22. The ripple in these patterns is caused by the small aperture size, and the asymmetry occurs because the element used for measurement was displaced one-half element from the aperture center. Averaged patterns (averaging out the pattern ripple) in the H-plane are seen to correlate well with predicted performance. The patterns with WAIM are broader than those without, particularly at 0.75 GHz, and better approximate the cos θ pattern. E-plane patterns, for which no predictions were made, are seen to be close to the cos θ pattern both with and without WAIM. No indication of undesirable aperture resonance (pattern notch) was observed in either scan plane over the operating band of 0.5 to 1.0 GHz. The broadside cross polarization component at 0.75 GHz was measured to be less than -27.4 dB.
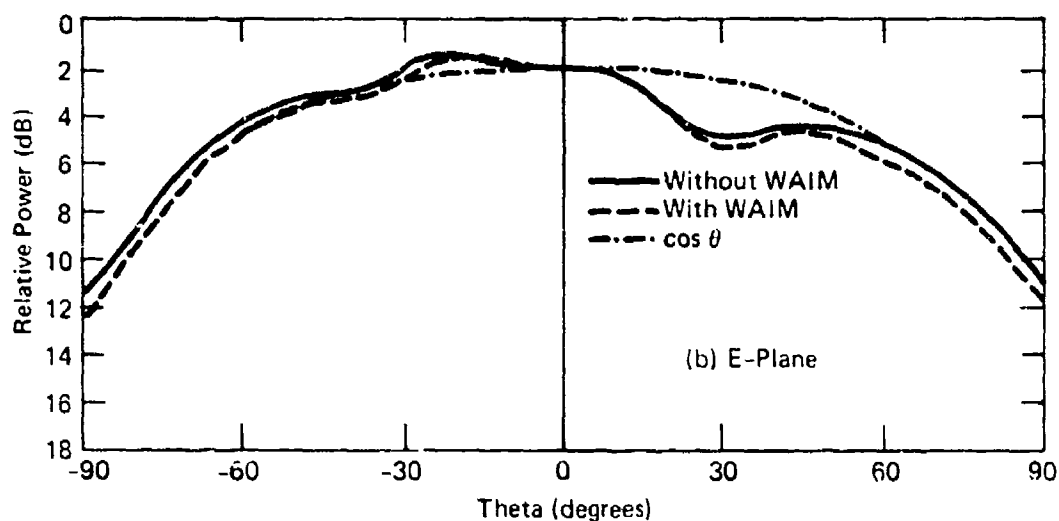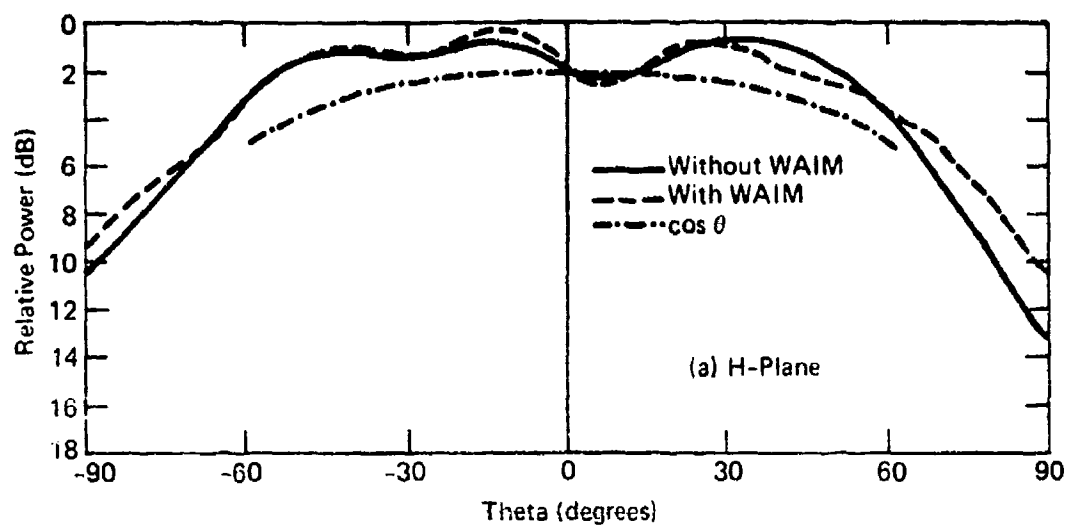
Fig. 20 H- and E-Plane Element Patterns, 10 by 10 Array, Frequency=0.5 GHz
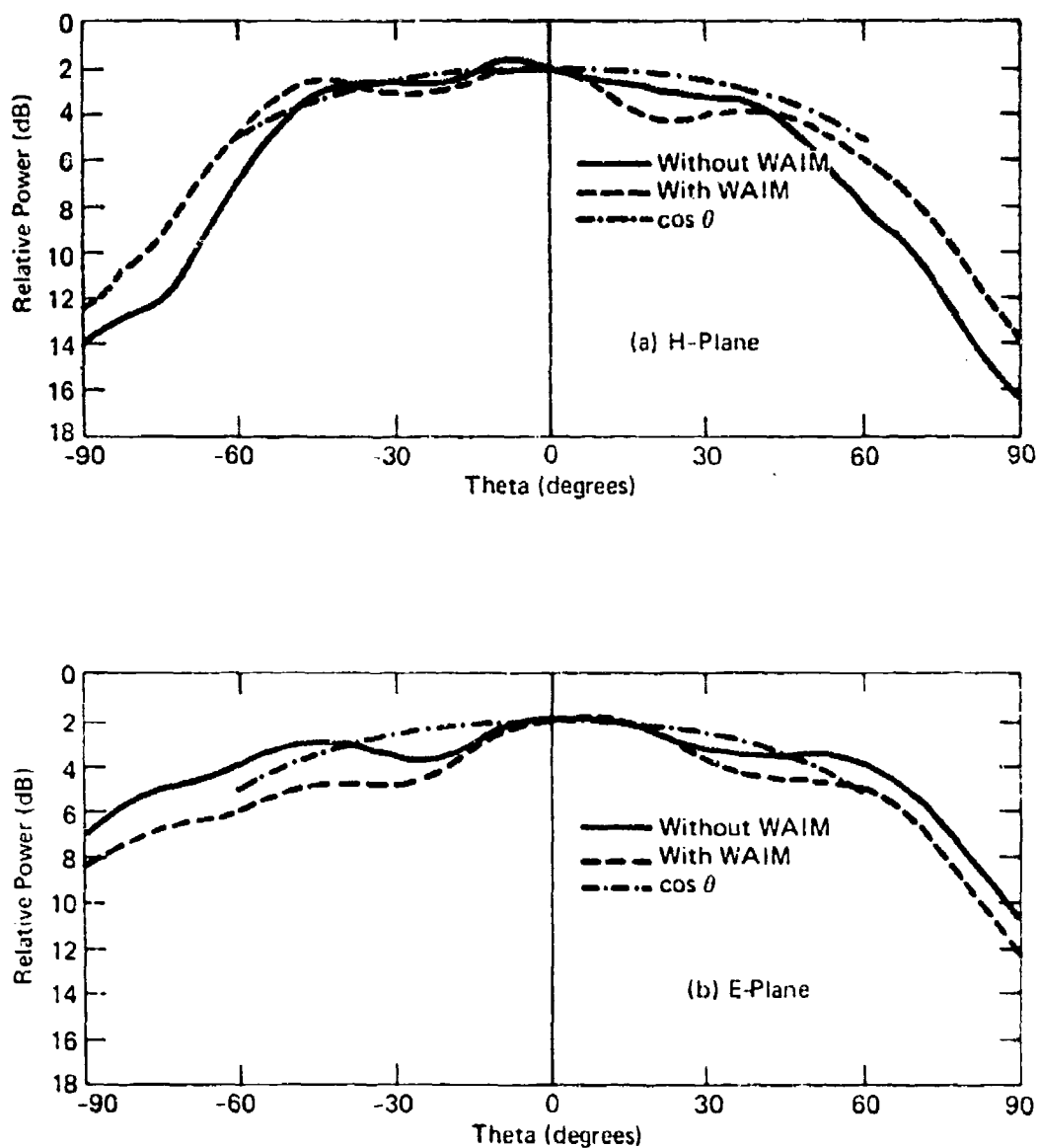
Fig. 21 H- and E-Plane Element Patterns, 10 by 10 Array, Frequency=0.75 GHz
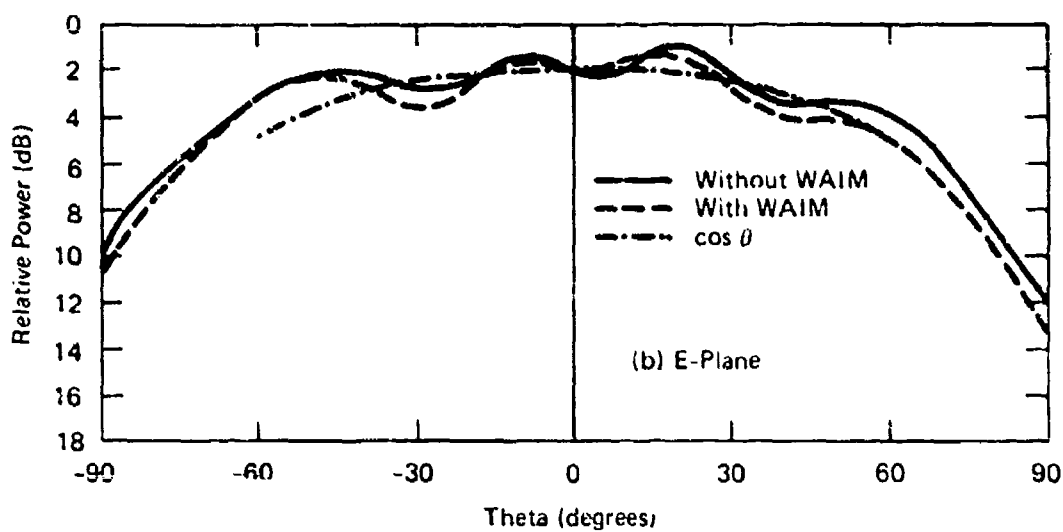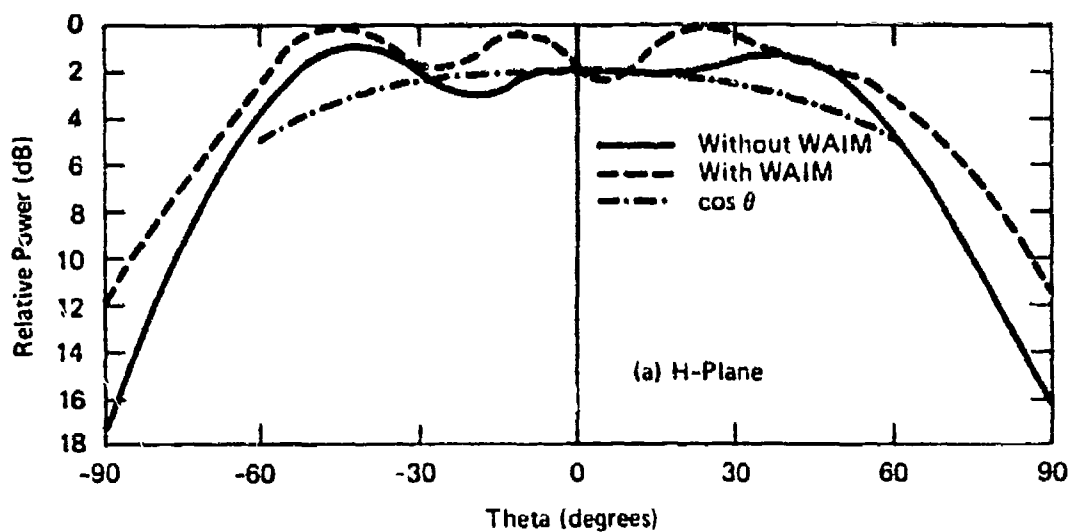
Fig. 22 H- and E-Plane Element Patterns, 10 by 10 Array, Frequency=1.0 GHz

3. WIDEBAND TRANSISTOR POWER AMPLIFIERS

AMPLIFIER DESIGN METHOD

The RF generating sources for the experimental solid-state array are microwave transistor amplifiers operated in the high efficiency class C mode. Operation in the class C mode has the unfortunate property of limiting instantaneous bandwidth in single transistor amplifiers to less than an octave. Harmonic frequencies present in the output waveform must be filtered by a less-than-octave passband filter. The filter is normally inherent in the amplifier output circuit.

Wideband class C power amplifiers at microwave frequencies require design methods substantially different from those used in small signal, class A designs. In small signal designs, "s"-parameter characterization is applicable, and the input and output impedance matching networks can be considered jointly in meeting design objectives. Characterization by " "-parameters is not applicable in class C designs because of the nonlinear operation, and the input and output networks must be considered separately. The output matching circuit is designed to achieve good efficiency and saturated output power over the bandwidth. The output circuit also affects power gain, which is often in conflict with output power objectives, and significantly affects the amplifier input impedance. Input circuitry is primarily directed at maximizing or leveling the amplifier gain over the required bandwidth.

The output circuit is designed first in class C power amplifiers with the objective of achieving a specified saturated output power at maximum efficiency. An approximation for the required load conductance is arrived at by using the expression given in Appendix E (Eq. (E-5)) for saturated output power:

$$P_{RF} = \frac{1}{2} (V_{cc} - v_{sat})^2 G_L .$$

The term v_{sat} is not a well defined quantity with microwave transistors and must be determined experimentally. DC-RF efficiency is affected by the susceptance of the load and, from Appendix E (Eq. (E-10)), is approximated by

$$\varkappa_c = \frac{\pi}{4} \frac{V_{cc} - v_{sat}}{V_{cc}} \Big/ \sqrt{1 + (B_L/G_L)^2} \quad .$$

Thus, the ranges over which the load conductance and susceptance are allowed to vary for a given output power and efficiency specification can in principle be defined.

In reality the approximations of Eqs. (E-5) and (E-10) do not yield reliable results because of complex parasitics and an ill-defined threshold of saturation in microwave transistors. The experimental procedure in designing an amplifier is to start with a load as determined from the approximations and then to tune the load to achieve the desired power and maximum efficiency at several frequencies across the band. After the optimum loads at several frequencies across the band are found, an output circuit is designed to approximate as closely as possible the optimum load.

The input circuit is designed to impedance match the transistor with the transistor connected to the previously designed output circuit since it affects the input impedance. Maximum gain with the given load results when the input is matched. If gain leveling is desired, selective mismatching is designed into the circuit. The procedure used in designing the input circuit is to impedance match the input with stub tuners at each of several frequencies across the band while keeping the output power at the prescribed level. At each frequency, the input tuning is removed from the transistor, and its impedance is measured "looking back" from the transistor. The measured impedance is appropriately transformed to the transistor input. The input circuit is designed to approximate the transformed optimum impedance across the frequer band.

WIDEBAND UHF AMPLIFIERS

The transistor selected for the amplifiers in the experimental wideband solid-state array is the TRW series MRA 0610-3 which is rated at 3 watts output with 50% efficiency and 10-dB gain over a 0.6 to 1.0 GHz band. This transistor has a built-in compensation network at the input to help impedance match parasitics and increase bandwidth. As with most microwave power transistors, the MRA 0610-3 is operated in a grounded base configuration. It is worth noting that an 18-watt version with the above bandwidth capability is also available.

We purchased an initial supply of TRW transistors, constructed input-output circuits (using a TRW design), and built a prototype amplifier in microstrip. A schematic circuit of the amplifier is given in Fig. 23, and the load admittances are shown in Fig. 24. The approximate load objective is calculated from Eq. (E-5) for 3 watts out assuming $v_{sat} = 7.5$ (Ref 14) and a transistor output capacitance of 4.5 pF. Admittances from the circuit were calculated using the output circuit in the schematic. Measured performance of the prototype amplifier is shown in Fig. 25; Fig. 26 is a photograph of the amplifier. These results are at the highest efficiency states. The output power is greater than 3 watts, gain more than 10 dB, and efficiency above 50% from 0.6 to 0.95 GHz. Satisfactory performance extends down to 0.55 GHz and up to 1.0 GHz.

A number of the TRW transistors were then purchased to satisfy the need for 18 amplifiers in the solid-state array (including the distribution network). The amplifiers were built using the RF circuit of the prototype

Ref. 14.   W. H. Leighton, R. J. Chaffin, and J. G. Webb, "RF Amplifier Design With Large Signal S-Parameters," IEEE Transactions on Microwave Theory and Techniques, Vol. MTT-21, December 1973, pp. 809-814.
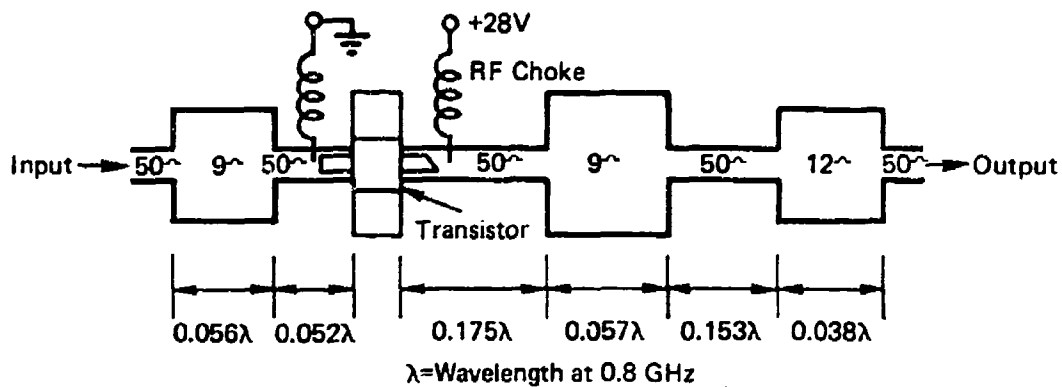
Fig. 23 Schematic Circuit of the Prototype Amplifier
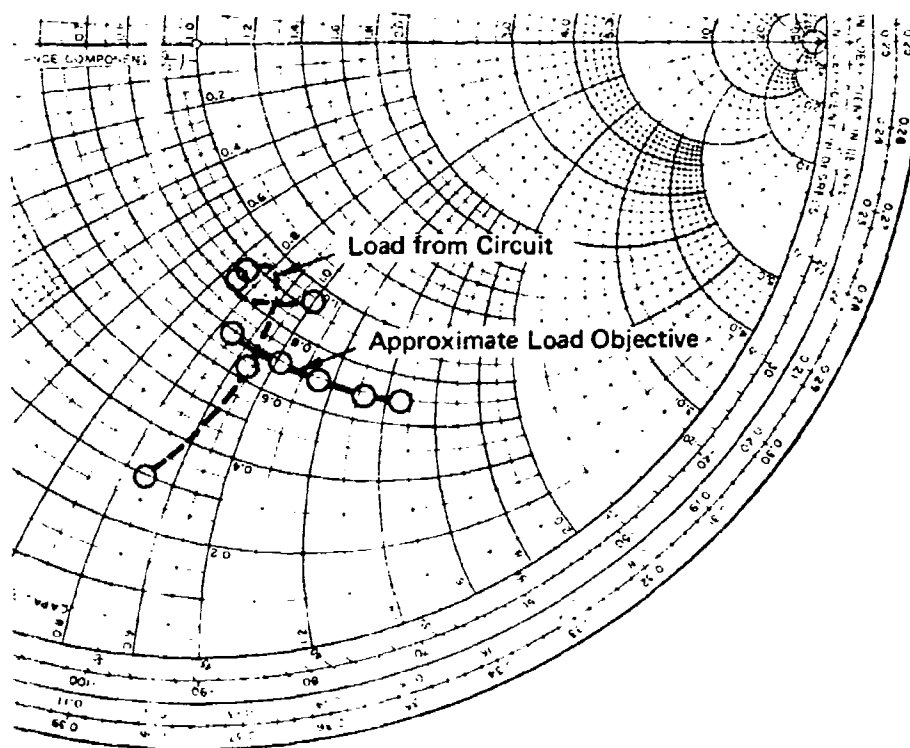
Fig. 24 Load Admittance of the Prototype Amplifier
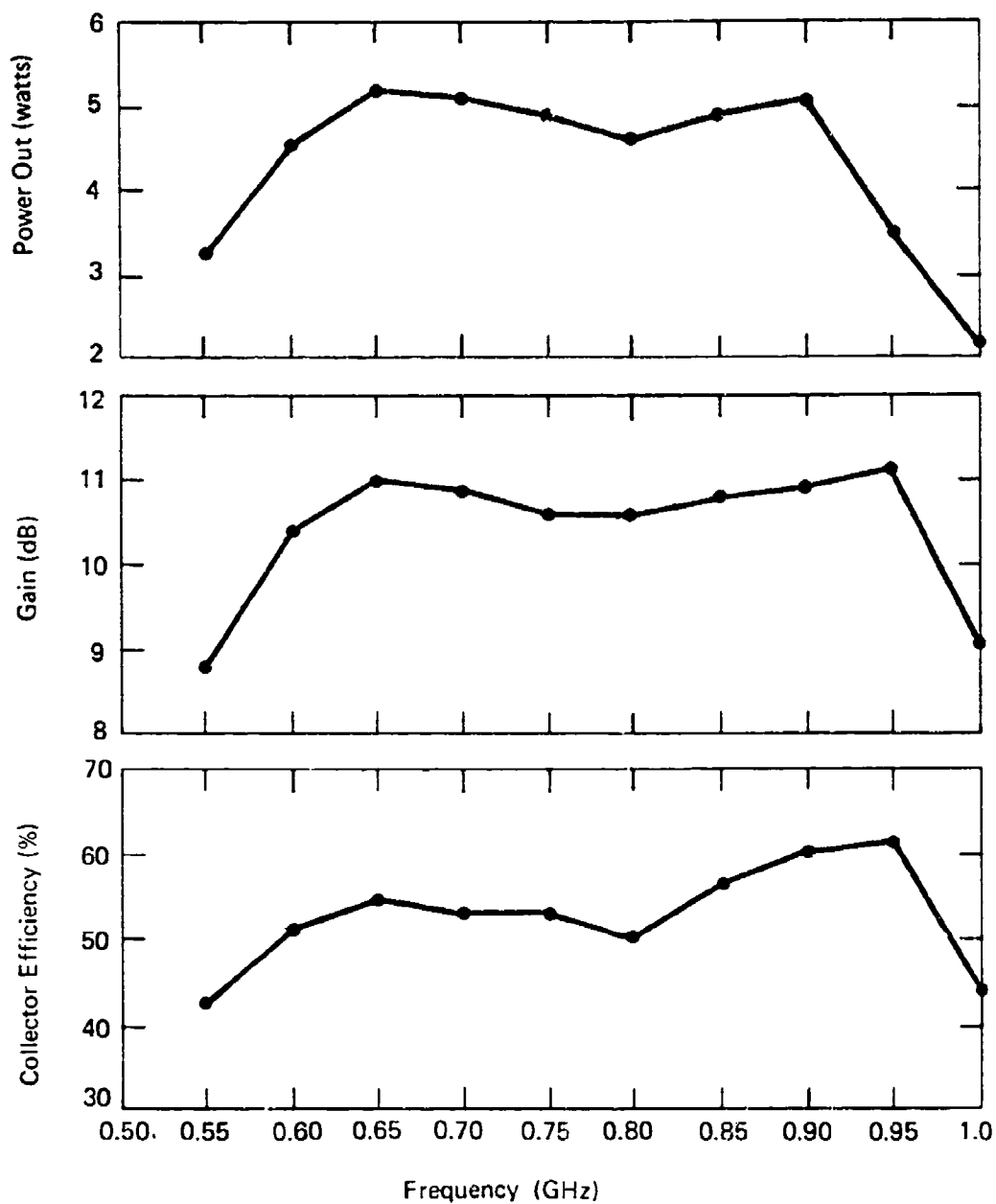
Fig. 25 Performance Data of the Prototype Amplifier
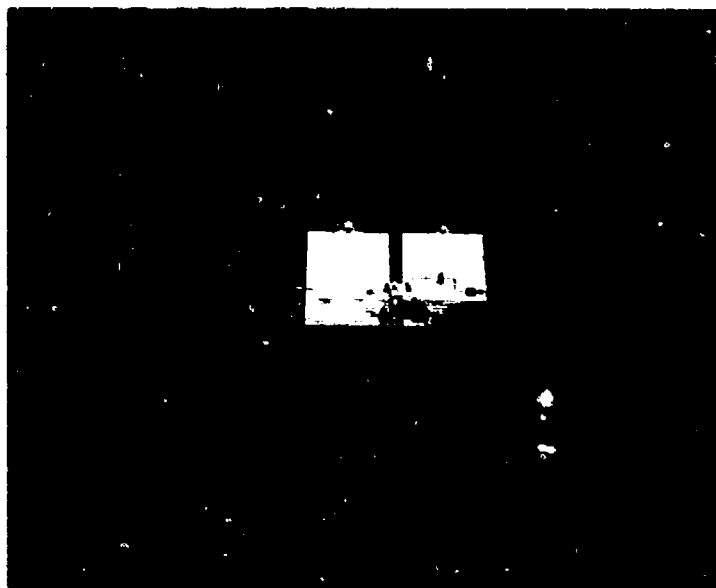
Fig. 26 The Prototype Amplifier

with specially designed circuit frames. Figure 27 is a
photograph of a typical amplifier. The output circuit was
built on a 99.5% alumina substrate 1 by 3 by 0.025 inches
with a 0.000 010 inch surface finish. Conductor metalliza-
tion is 0.000 250 inch of gold on top of a chrome bonding
layer 10 nm thick. The input circuit was built on an iden-
tical substrate 1 by 1 inch thick.

Measurements performed on the several amplifiers
showed performance that was significantly different from
that obtained with the prototype; in all cases performance
was degraded. The difference is attributed to variations
in transistors from batch to batch and differences in pack-
age parasitics possibly due to changes in fabrication
methods, personnel, or normal uncontrollable variations
in the fabrication process. Since the input-output circuits
were designed around the transistor used in the prototype,
it is not surprising that performance was degraded in all
others.
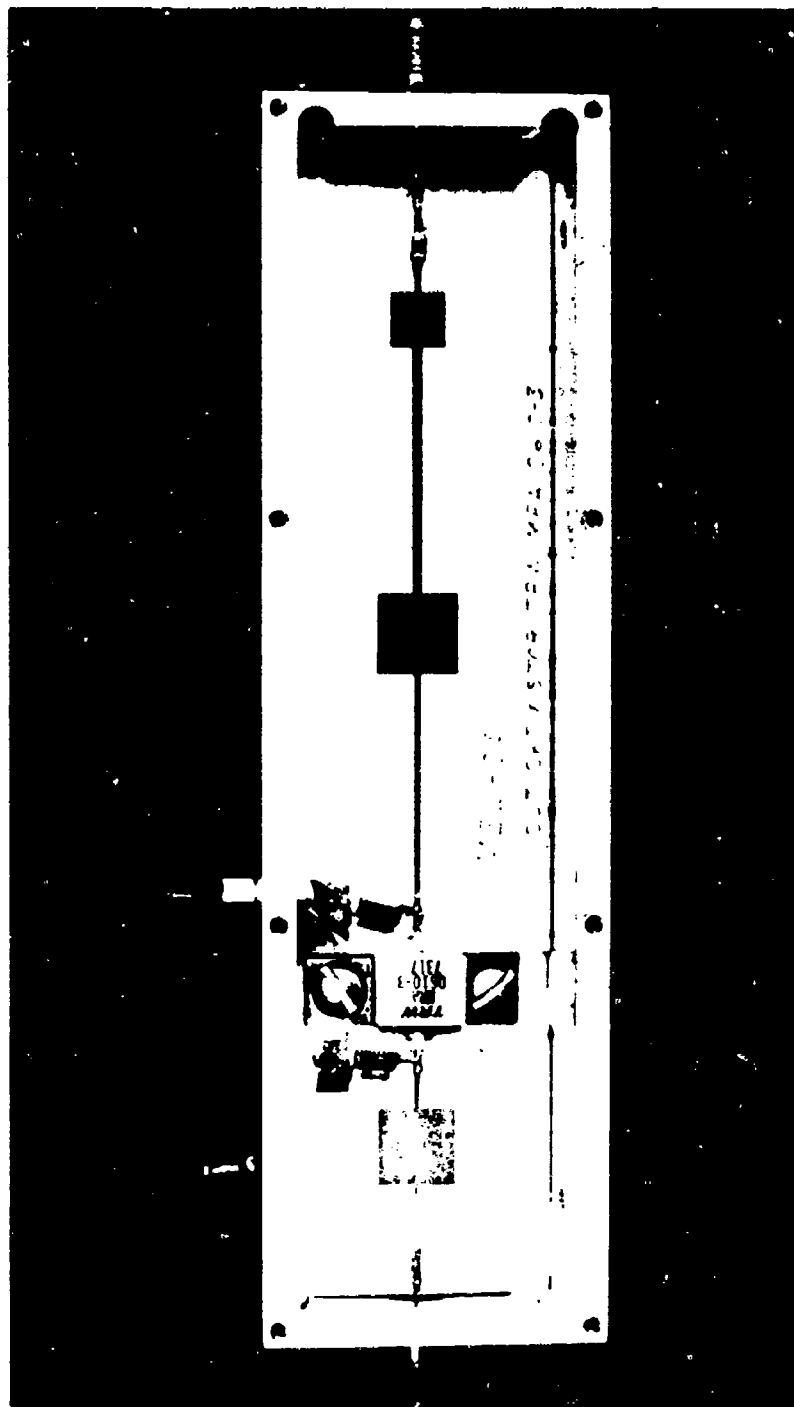
Fig. 27   Wideband RF Amplifier for Solid-State Array

Due to this degraded performance, it was necessary to modify the circuits, to the extent that this could be easily accomplished, to bring performance to an acceptable level. Modification was done by placing capacitive pads of conductive silver paint at judiciously selected positions along the circuits. Trial and error methods were used, and nearly every circuit required different modification.

The final performance of the several amplifiers is shown in Fig. 28 where the shaded region is the performance variation. The most pronounced variation is in amplifier gain where there is as much as 3.6 dB difference at a single frequency and 3.8 dB across the 0.6 to 0.95 GHz band. Relative phase shift of the several units is also shown. The maximum phase difference between units is 41° at 0.6 GHz and the minimum is 29° at 8.0 GHz. The maximum and minimum rms phase errors with all amplifiers is 14.5° (0.25 rad) and 7.9° (0.14 rad), respectively.
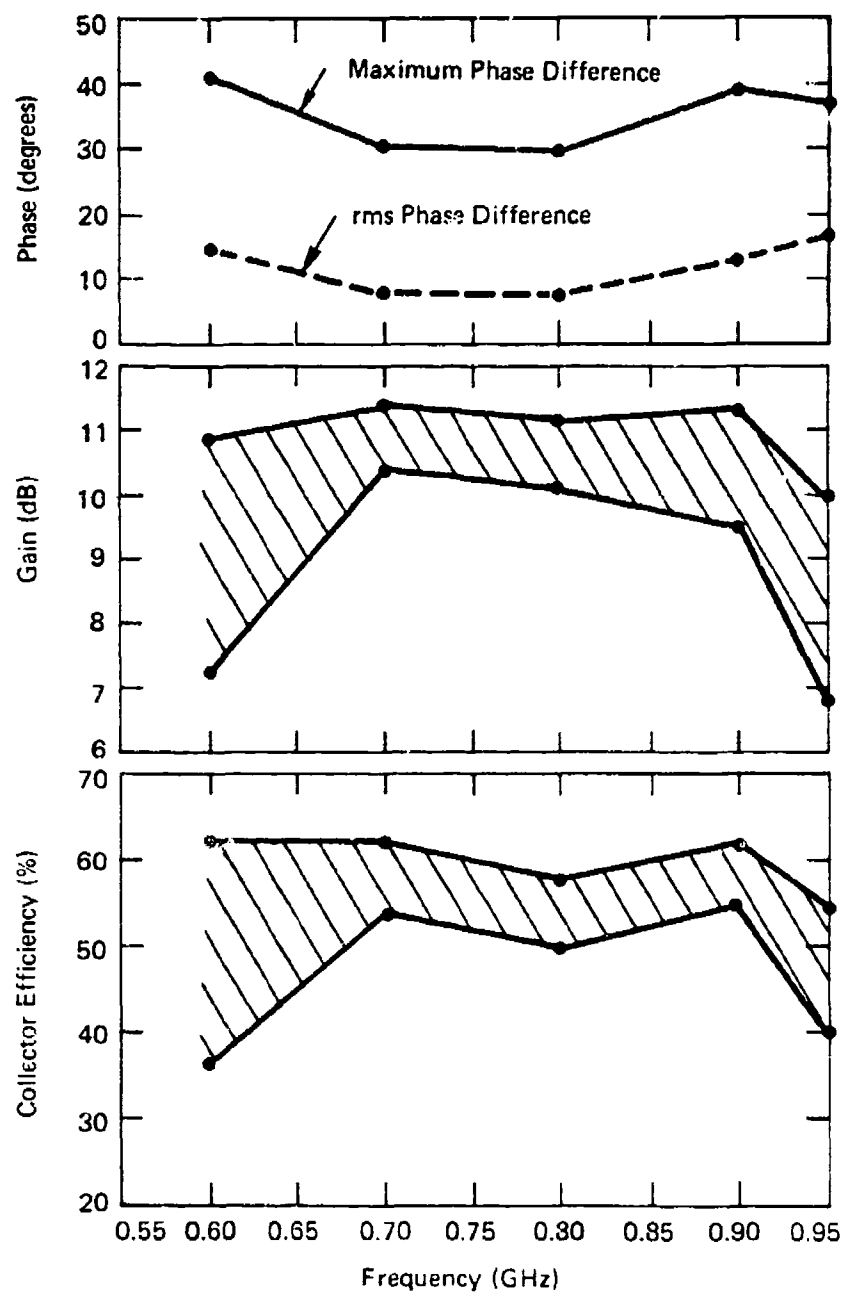
Fig. 28 Final Performance of the RF Amplifiers

4. INTEGRATED ANTENNA SYSTEM

A 16-element linear array aperture of the printed circuit radiators and several transistor amplifiers were integrated to form an array system with experimental very wideband solid-state characteristics: it is shown schematically in Fig. 29. Dimensions of the aperture (without the WAIM sheet) are given in Fig. 30. Performance objective was beam scanning to $\pm 60°$ in the H-plane over a 0.6 to 0.95 GHz band (the amplifiers capacity was the limiting factor).
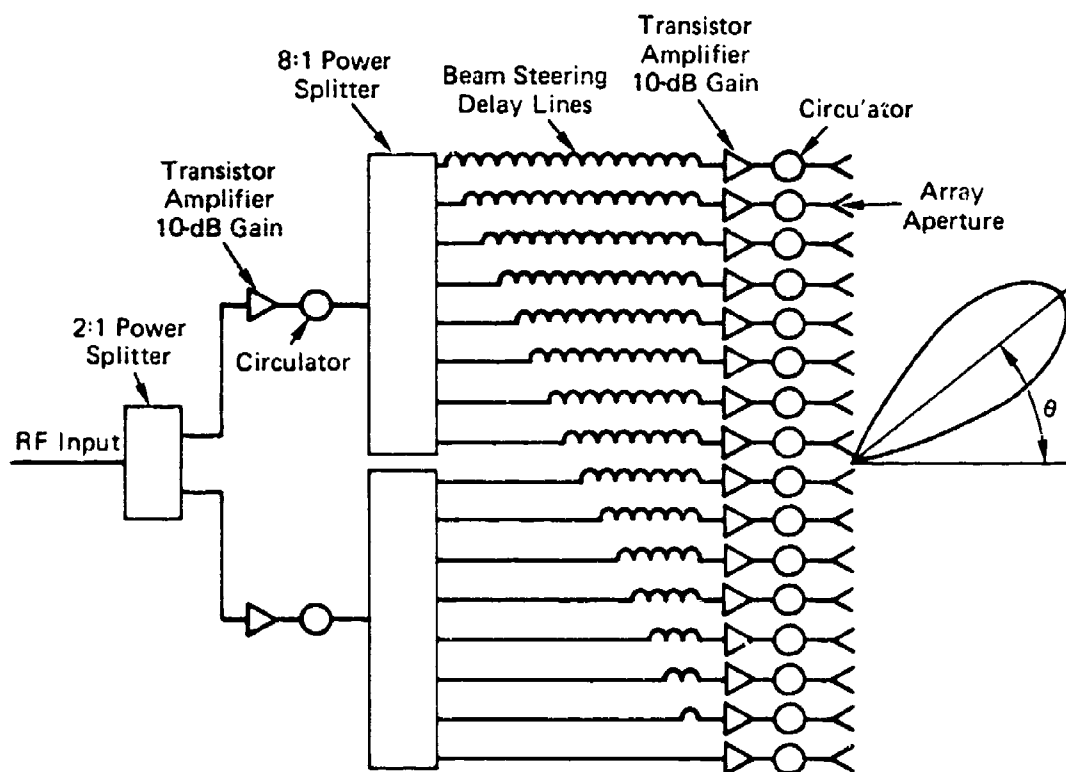
Fig. 29 Schematic of the 16-Element Solid-State Array System

All Dimensions Are in Inches

60.00

Ground Plane

Feed Probes

$\epsilon_r=2.5$

3.75

Conducting Strip

2.75

3.00

1.50

3.75

Dielectric

Fig. 30 Dimensions of the 16-Element Linear Array Aperture
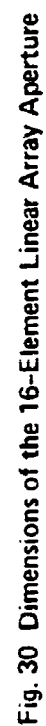
A large planar array was simulated in the nonscanning E-plane (to maintain aperture impedance match) by placing the linear array aperture between parallel conducting planes spaced by the E-plane element spacing of the simulated array. Elements are imaged in the planes in a fashion identical to that in a waveguide simulator. The ends of the array were closed off and the enclosure flared out into a horn for radiation into space. To minimize horn aperture reflections (VSWR < 1.5:1), the E-dimension (24 inches) of the horn was chosen to be greater than one wavelength at the lowest frequency. The E-plane horn angle of 23° minimizes horn throat reflection (VSWR < 1.5:1). H-plane scanning to 60° required that the H-plane horn angle be ±60°. Horizontal space limitations in the anechoic chamber used for the measurements forced the horn to be built in two parts. A basic section was built with ±30° H-plane flares permitting scanning to ±30°. A wing extending one side to 60° was attached for scanning between 30° and 60°. In the latter configuration, the array had to be set off-center on the chamber pedestal in order to be accommodated in the anechoic chamber. Figure 31 is a photograph of the array system mounted on the pedestal in the chamber.

Each radiating element in the array was driven by a 0.6 to 0.95 GHz bandwidth transistor amplifier. The several amplifiers were arranged in the array according to gain such that, at midband, higher gain amplifiers were in the array center and lower gain units at the edges. Amplifier gains vary with frequency as well as from unit to unit, resulting in the aperture amplitude errors given in Fig. 32. The outputs of the amplifiers were protected from aperture mismatch by isolators.

The distribution network for the experimental array was a matched 16:1 power divider assembled from 180° hybrids. This type of manifold provides isolated feeds to the RF drive amplifier at the elements, thus eliminating aperture illumination anomalies due to amplifier input mismatch (i.e., a reactive feed network has an output power distribution strongly dependent on load mismatch). Two RF
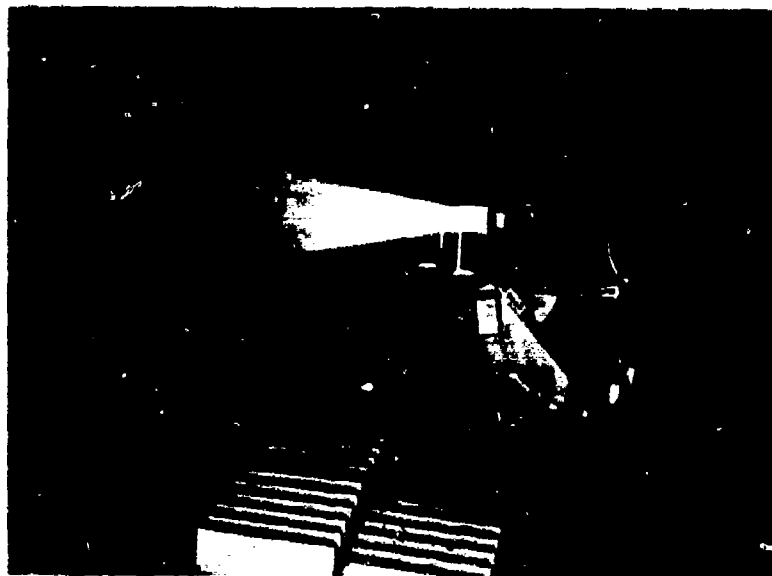
Fig. 31 16-Element Integrated Linear Array System Mounted on Pedestal in Anechoic Chamber
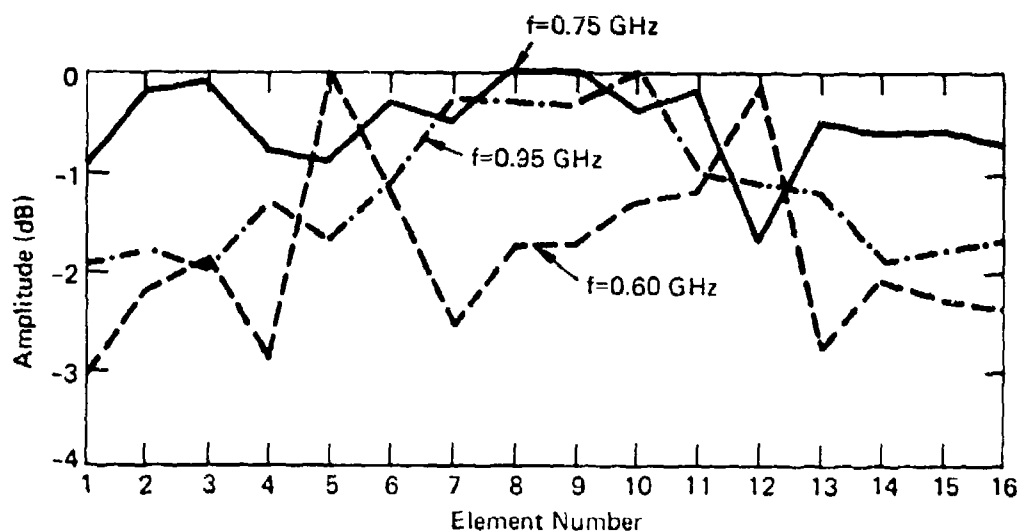
Fig. 32 Aperture Amplitude Variation due to Amplifier Gains

amplifiers were used within the feed network to supply RF power to the drive amplifiers.

Beam steering, confined to the H-plane, was accomplished by inserting lengths of time-delaying coaxial cables between the feed network and integrated array elements. Cable sets were procured for the scan angles of 0°, 15°, 30°, 45°, and 60°.

Antenna pattern measurements on the integrated array were made in an anechoic chamber at the APL Antenna and Boresite Facility. Patterns at 0.6, 0.75, and 0.95 GHz for the H-plane scan angles of 0°, 30°, and 60° are given in Figs. 33, 34, and 35. The 0° and 30° beams show beam widths and sidelobe levels approximately as expected. The lack of sharp nulls between sidelobe is due to phase error between driver amplifiers at each radiating element, and is particularly pronounced at 0.6 GHz where the maximum phase error exists. The asymmetry in the broadside patterns is due to phase error between amplifiers with the two amplifiers in the feed distribution network probably contributing the most significant effect.

Measured antenna gain as a function of frequency is plotted in Fig. 36. Broadside gain is given for the solid-state array, and gain variation with scan angle is given for the antenna without amplifiers (passive). The reference gain is for an assumed effective antenna aperture equal to the array length (60 inches) times the enclosing horn height (24 inches). The observed rolloff in the broadside solid-state array gain at the high and low frequencies is due to variation in transistor amplifier gains. As discussed previously, the amplifier gains are maximum at midband and roll off by as much as 3.8 dB at the band edges. In the experimental solid-state array the rolloff is approximately twice that of a single amplifier since the amplifiers in the distribution network also have low gains at the band edges.

An unexpected result from the antenna measurements is the low gain measured at 60° when the antenna is
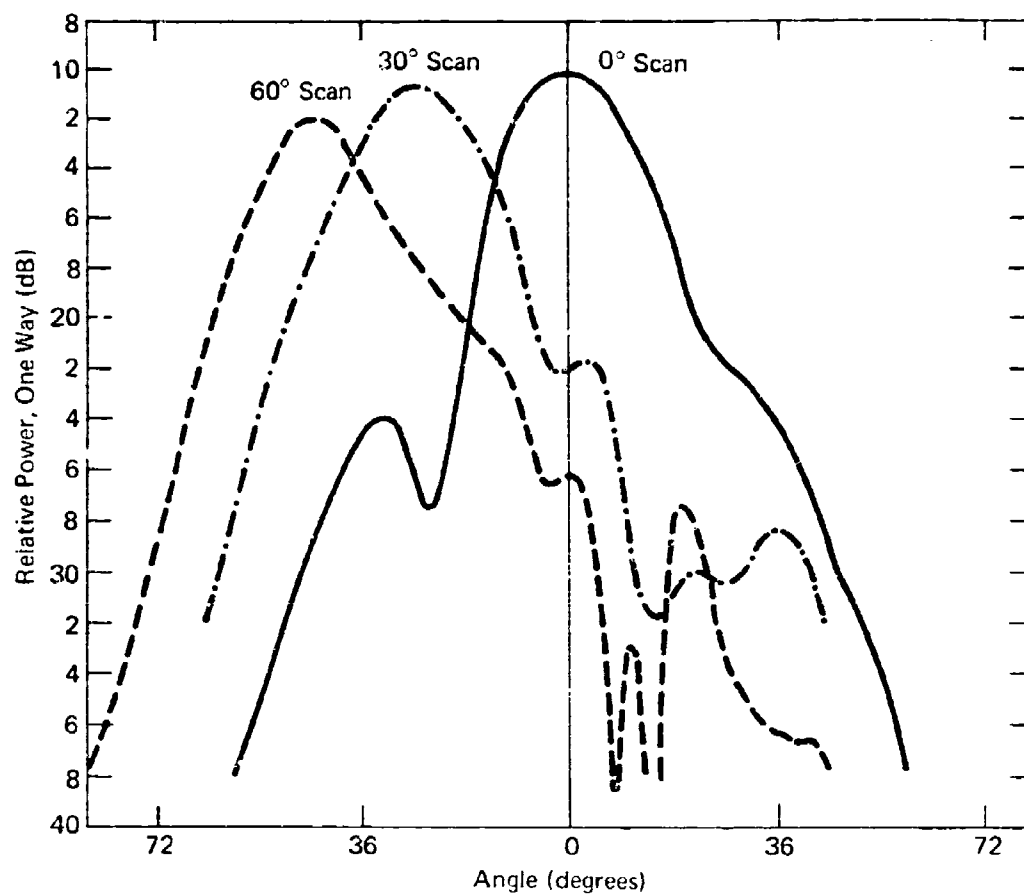
Fig. 33 Antenna Patterns, 16-Element Integrated Linear Array, Frequency=0.6 GHz
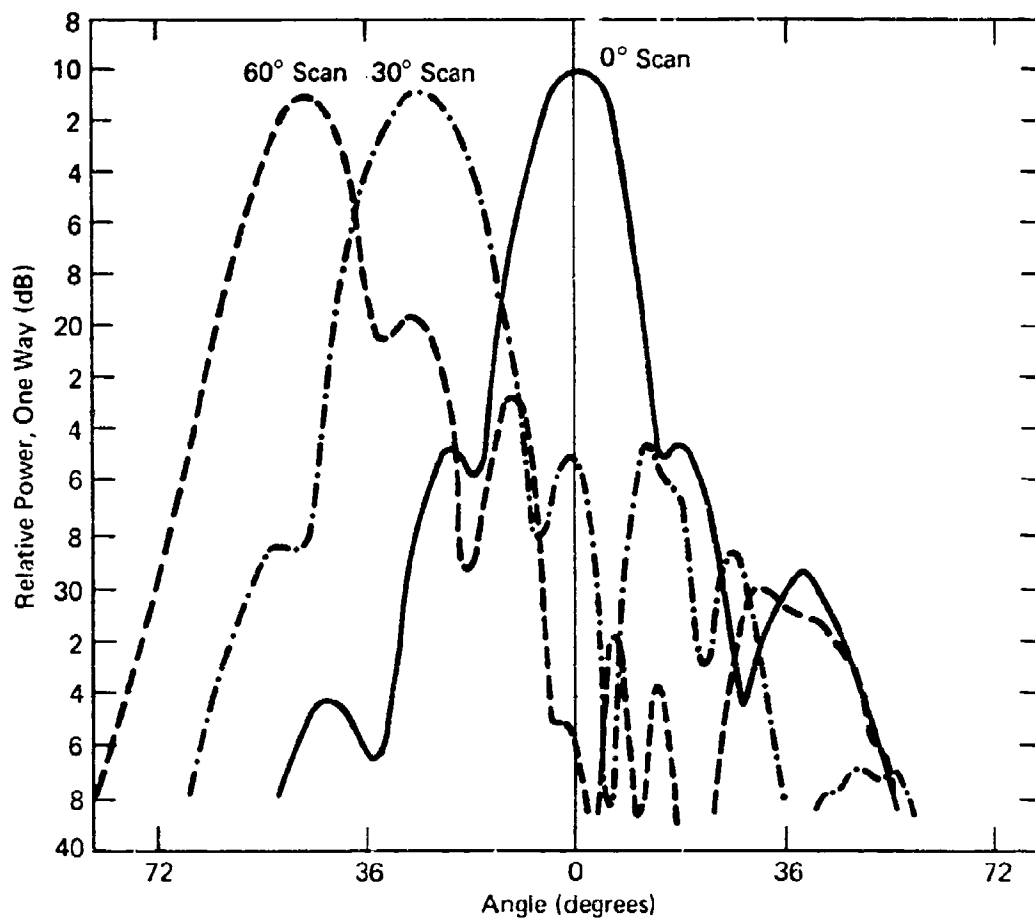
Fig. 34 Antenna Patterns, 16-Element Integrated Linear Array, Frequency=0.75 GHz
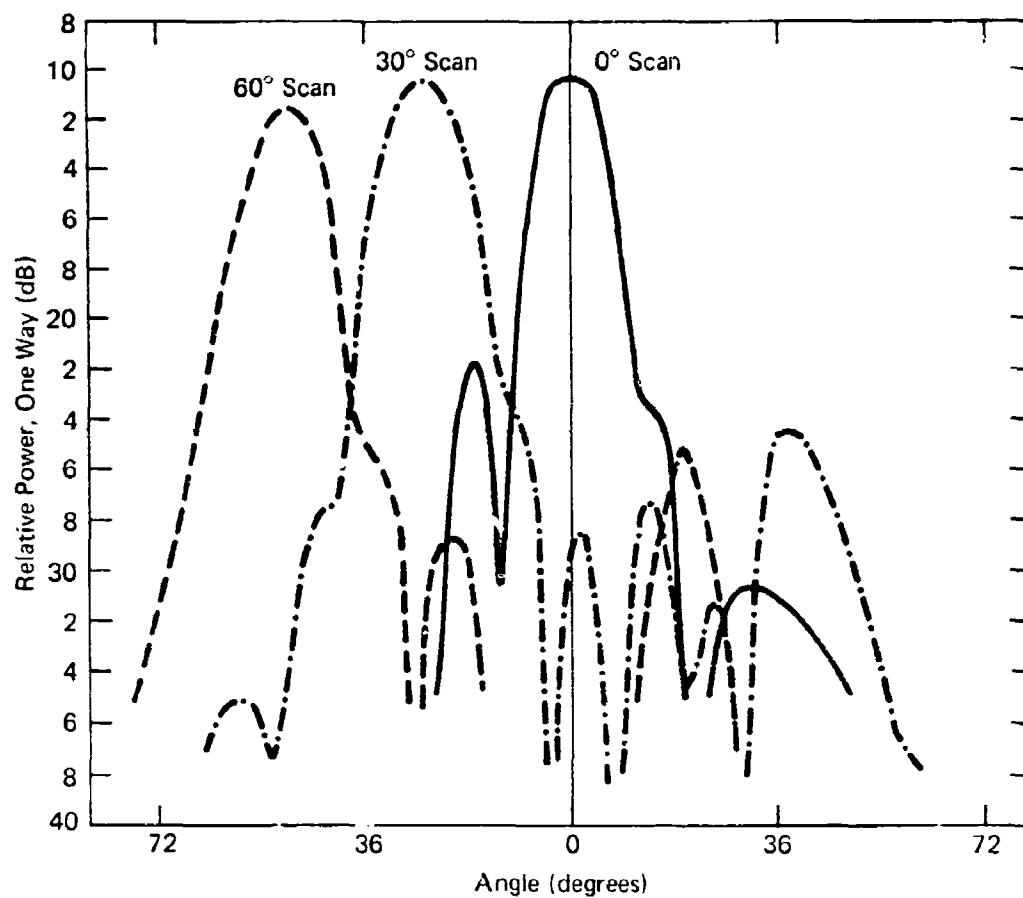
Fig. 35 Antenna Patterns, 16-Element Integrated Linear Array, Frequency=0.95 GHz
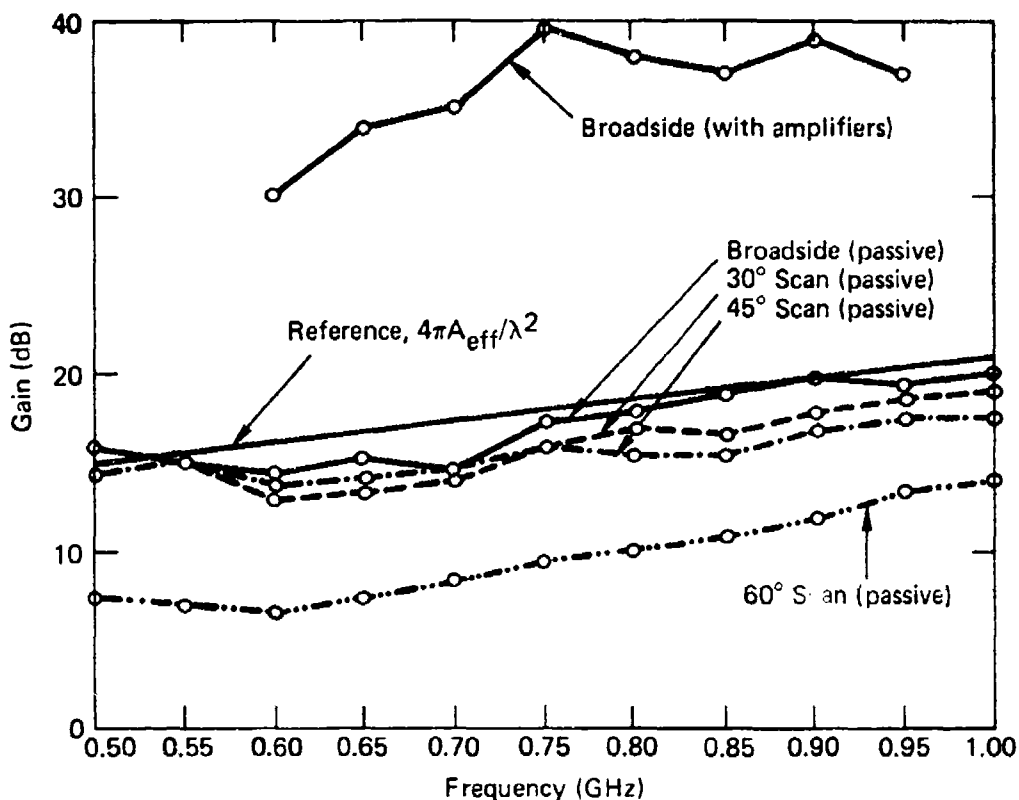
Fig. 36 Gain of 16-Element Linear Array

phased to a pointing angle of 60°. Also, the measured
beam patterns at this phasing have maxima at angles
smaller than anticipated and excessively high sidelobes.
These results are, of course, indicative of narrow element
patterns. Since broad element patterns were measured
with the 10- by 10-element aperture, it was felt that the
anomalous behavior might be caused by shadowing from the
enclosing sidewalls of the horn. To verify the hypothesis,
two sets of element patterns with the linear array were
measured at 0.95 GHz. The first set was measured on the
aperture enclosed in the horn with the 30° H-plane flare

- 57 -
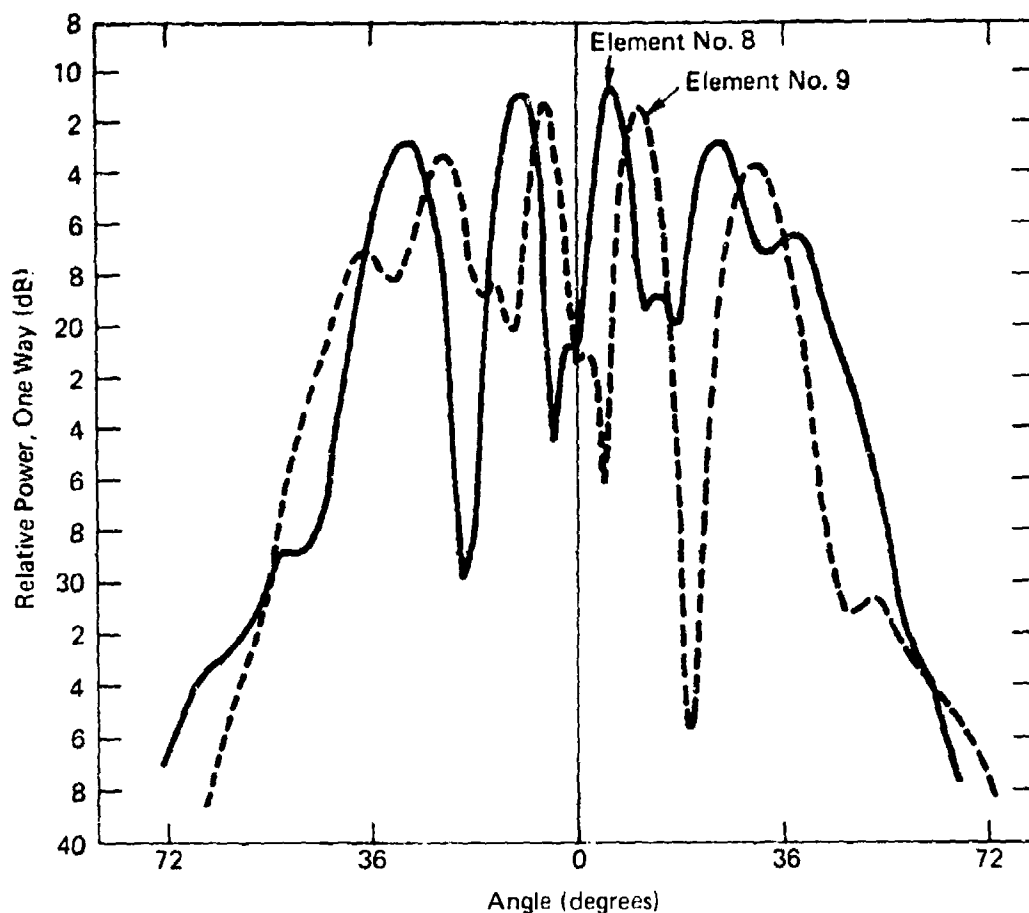
Fig. 37 Element Patterns, 16-Element Linear Array Enclosed in Horn,
Frequency=0.95 GHz

angles. Figure 37 shows the patterns for the two center
elements. Unfortunately, element patterns were not mea-
sured with the 60° wing attached, but the patterns given are
clearly much narrower than previously measured patterns
and show much evidence of severe pattern interference
from multiple reflections off the sidewalls. The pattern
interference tends to average out across the 16 elements,
which undoubtedly accounts for the behavior of gain versus
frequency and gain versus scan angle seen in Fig. 36.

The second set of patterns was measured with the horn removed, leaving the array enclosed in a 9-inch section of parallel plane with small flare and open ends. Figure 38 shows the patterns for the two center elements. These patterns are very broad, demonstrating that the horn enclosure is the cause of the narrow element patterns, low $60°$ gain, and beam maxima occurring at small angles.

In conclusion, the experimental solid-state array has beam steering capability to $\pm60°$, but the presence of the enclosing horn which was used to maintain aperture impedance match caused the high scan angle beams to deteriorate. It should be emphasized that the horn was a measuring tool and would not be used in an operational array. Further, it is apparent from these observations that future experimental arrays of this nature should not be enclosed in a horn but rather should be surrounded with terminated dummy elements.
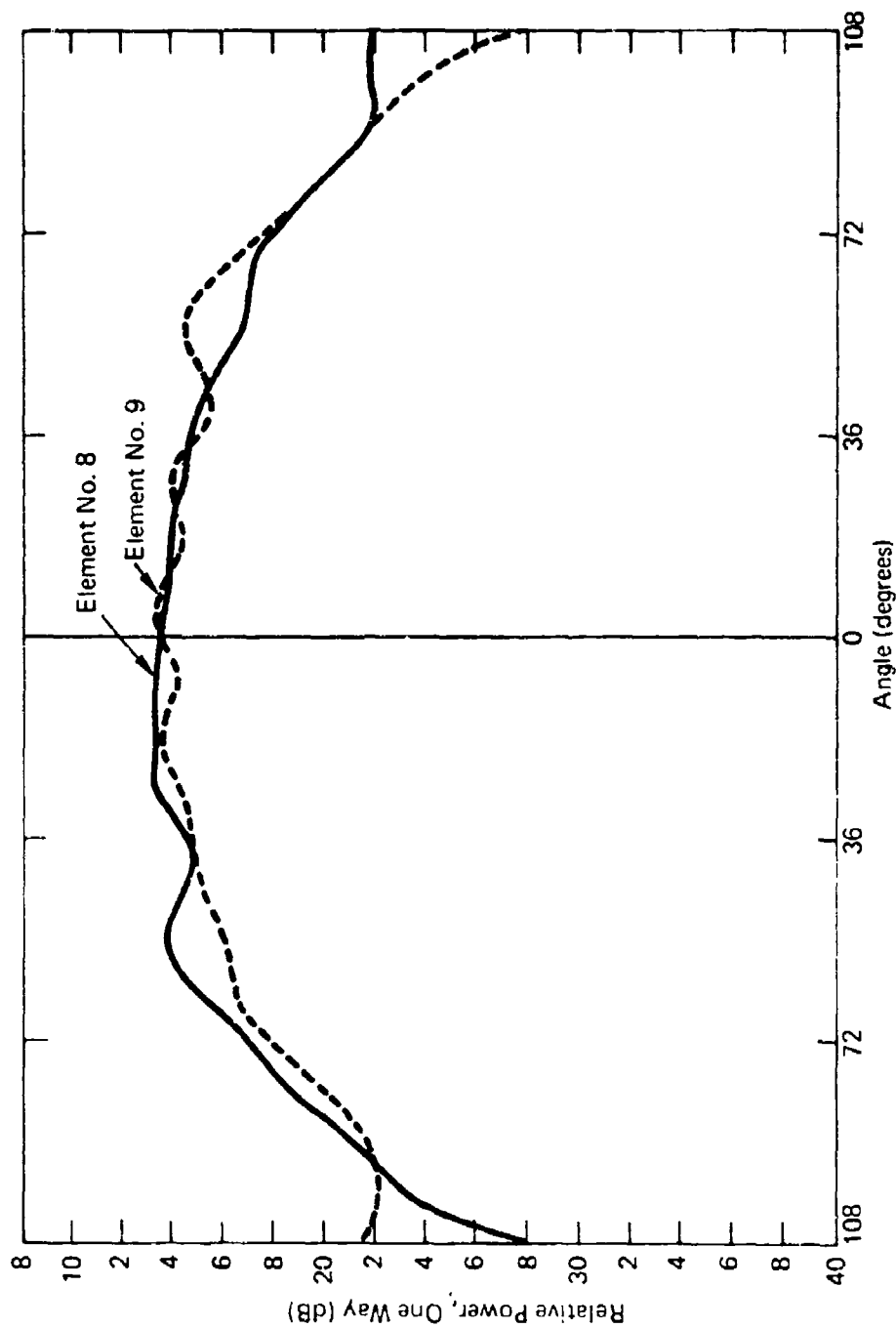
Fig. 38 Element Patterns, 16-Element Linear Array, Horn Removed, Frequency=0.95 GHz

5. SUMMARY AND CONCLUSIONS

We developed and tested a phased-array aperture impedance matched over an octave bandwidth and with beam scanning to ±60°. The aperture, consisting of strip radiators, was modeled, and design curves were generated. Predicted performance of the aperture was a VSWR under 3.0:1 over a 0.5 to 1.0 GHz frequency band with scanning in the H-plane to 60°. Experimental data from measurements in a waveguide simulator have demonstrated a close fit with predicted data. A 10- by 10-element aperture was built to measure element patterns in the E- and H-planes; these patterns were close to the cos θ shape out to 60° in both planes over the octave band. The aperture design is attractive for solid-state array application in that it is made with printed circuitry and lends itself to interfacing with integrated circuits.

Wideband transistor amplifiers, using TRW MRA 0610-3 transistors operating in class C, were built and evaluated for use as RF sources in a solid-state array. Performance of a prototype amplifier was greater than 10-dB gain at more than 50% efficiency for power levels in excess of 3 watts over a 0.6 to 0.95 GHz band. When a large number (more than 18) of the amplifiers were built, it was found that amplifier performance was significantly degraded due to variations in transistor characteristics. As a result none of the amplifiers achieved the performance of the prototype, and each amplifier had to be individually tuned. This experience suggests that current transistor manufacturing methods are unable to mass produce transistors sufficiently similar for wideband high power transistor circuits without individual tuning.

A linear array aperture of the radiating elements was integrated with the wideband transistor amplifiers to form a wideband solid-state phased-array system. Beam scanning, by means of inserting lengths of coaxial delay

lines between the antenna and a feed network, is to $60°$ in the H-plane. Antenna performance was measured in an anechoic chamber over the 0.6 to 0.95 GHz frequency range (transistor amplifiers are the limiting factor). Satisfactory beam patterns were obtained for scan angles out to $30°$, but patterns further out were less than satisfactory due to pattern deterioration from the enclosing horn.

This developmental effort demonstrates that wideband solid-state phased-arrays are feasible. Matched octave band array apertures with wide angle scanning are within the current state of the art. Wideband transistor amplifiers are also available, but experience indicates that mass production is a problem. In addition, the amplifiers used in this effort are inherently limited to less than an octave bandwidth (due to class C operation). A full octave, or greater, solid-state array would require further development in transistor amplifiers to achieve octave bandwidth circuits.

Appendix A

EQUIVALENT CIRCUIT FOR ARRAY OF STRIP RADIATORS

The equivalent circuit for an array of strip radiators is developed from a model that considers the array aperture simulated in waveguide, as was shown in Fig. 3. The height of the waveguide simulator is one-half the E-plane spacing so that only a single feed probe of each element is included. However, multiple probes in the H-plane can be included. As described in the body of the text, the model views the air-filled simulator and the aperture dielectric region as separate waveguide sections coupled by a slit. An array of feed probes excites fields in the dielectric region (horizontal E-fields in Fig. 3), and a short circuited length of guide is paralleled across the probes. The slit coupled region, the array of feed probes, and the short circuit guide section are treated separately in the following subsections: their equivalent circuits are then joined to form the array aperture equivalent circuit. It is assumed that the separation between these waveguide obstacles is sufficient so that coupling by means of fringing fields between them is negligible.

SLIT-COUPLED WAVEGUIDE SECTIONS

A portion of the strip radiator model consists of two waveguide sections coupled by a slit where one of the guides is filled with dielectric. The equivalent circuit of the coupling is developed by first considering the partially filled T-junction shown in Fig. A-1. The two rectangular guides are of unequal heights but equal width, and are coupled by a narrow slit across a wall of zero thickness. TE_{10} modes are assumed to exist in both guides. The equivalent circuit and element values for an air-filled

Guide Width = a

Side View   Equivalent Circuit
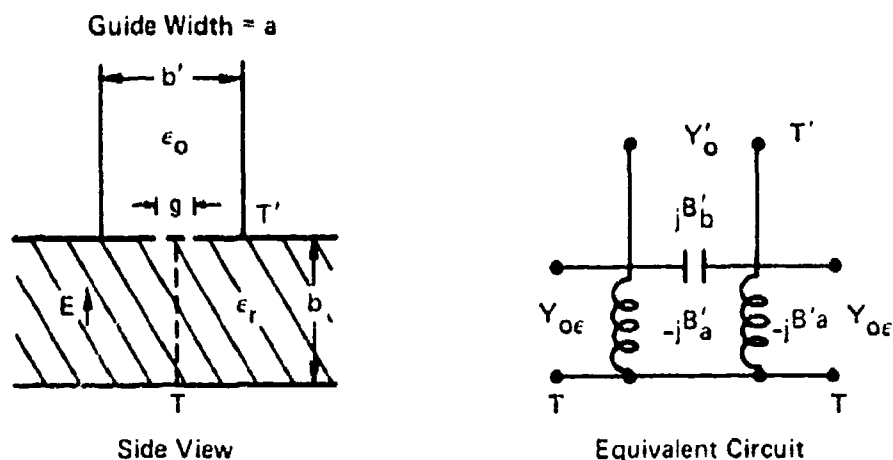
Fig. A-1 Partially Filled Slit-Coupled T-Junction

structure have been previously given by Marcuvitz (Ref. 15,
pp. 351-352). The form of the equivalent circuit is assumed
to be valid also for a fully filled structure and for the par-
tially filled junction shown on Fig. A-1. When both guides
are dielectrically filled, the element values are given rela-
tive to the filled guides and may be rewritten as

$$\frac{Y'_{o\epsilon}}{Y_{o\epsilon}} = \frac{b}{b'} \tag{A-1}$$

$$\frac{B_{a\epsilon}}{Y_{o\epsilon}} = \frac{b}{\lambda_{g\epsilon}} \left(\frac{\pi g}{4b}\right)^2 , \quad g \ll b \tag{A-2}$$

Ref. 15.   N. Marcuvitz, Waveguide Handbook, Vol. 10,
MIT Radiation Laboratory Series, New York: McGraw-
Hill, 1951.

$$\frac{B_{b\epsilon}}{Y_{o\epsilon}} \approx \frac{4b}{\lambda_{g\epsilon}} \left[\ln \frac{2\sqrt{2bb'}}{\pi g} + \left(\frac{b}{\lambda_{g\epsilon}}\right)^2 \right], \; b \ll \lambda_{g\epsilon} \qquad (A\text{-}3)$$

where

$$\lambda_{g\epsilon} = \lambda / \sqrt{\epsilon_r - (\lambda/\lambda_c)^2} \; .$$

To develop the equivalent circuit values for the partially filled T-junction, it is necessary to consider separately the small slit or symmetrical iris across a rectangular guide. The iris is represented by a capacitive susceptance (Ref. 15, pp. 218-219). As before, when the guide is dielectrically filled, the susceptance may be rewritten as

$$\frac{B_{c\epsilon}}{Y'_{o\epsilon}} = \frac{4b'}{\lambda_{g\epsilon}} \left\{ \ln\left(\frac{2b'}{\pi g}\right) + \frac{1}{6}\left(\frac{\pi g}{2b'}\right)^2 + \frac{1}{2}\left(\frac{b'}{\lambda_{g\epsilon}}\right)^2 \left[1 - \frac{1}{2}\left(\frac{\pi g}{2b'}\right)^2\right]^4 \right\}, \; g \ll b'$$

$$(A\text{-}4)$$

where

$$\lambda_{g\epsilon} \text{ is replaced by } \lambda_g$$
$$Y'_{o\epsilon} \text{ is replaced by } Y'_o$$

for air filled.

The equivalent circuit and element values of the partially filled T-junction can now be found from the completely filled T-junction and the symmetrical iris. The coupling slit between guides in the partially filled T-junction is assumed to be narrow so that in the plane of the slit only horizontal field components normal to the strip edges exist. Under this assumption the guide section above the reference plane T' is equivalent to one side of an air-filled guide with iris. It follows that the inductive components of the T-junction circuit are functions of the configuration below the reference plane and are unaffected by a change of dielectric

- 65 -

in the upper region. The total capacitance in the partially
filled junction is arrived at by subtracting one-half the
capacitance of a dielectric-filled guide with an iris from
the capacitance of a fully filled T-junction, and adding one-
half the capacitance of an air-filled guide with an iris:

$$B_b' = B_{b\epsilon} - \frac{1}{2} B_{c\epsilon} + \frac{1}{2} B_c \qquad (A-5)$$

$$\frac{B_b'}{Y_{o\epsilon}} = \frac{B_{b\epsilon}}{Y_{o\epsilon}} - \frac{1}{2} \frac{B_{c\epsilon}}{Y_{o\epsilon}'} \frac{Y_{o\epsilon}'}{Y_{o\epsilon}} + \frac{1}{2} \frac{B_c}{Y_o'} \frac{Y_o'}{Y_{o\epsilon}} \qquad (A-6)$$

where

$$B_a' = B_{a\epsilon} \quad \text{and}$$

$$\frac{Y_o'}{Y_{o\epsilon}} = \frac{b}{b'} \frac{\lambda_{g\epsilon}}{\lambda_g} \; .$$

The junction of particular interest in modeling the
array aperture of strip radiators is the bifurcated T-junc-
tion wherein only one-half of the above structure is con-
sidered. When the T-junction is excited by a TE_{10} mode
in the vertical guide, a conducting septum may be inserted
along symmetry plane T, as illustrated in Fig. A-2. Since
the septum is normal to all horizontal fields, and at the
plane of symmetry there are no vertical fields, the overall
field configuration is undisturbed. The resulting two L-
junctions are separable, and each has the equivalent cir-
cuit shown. Circuit values are given by

$$B_g = 2B_b' \qquad (A-7a)$$
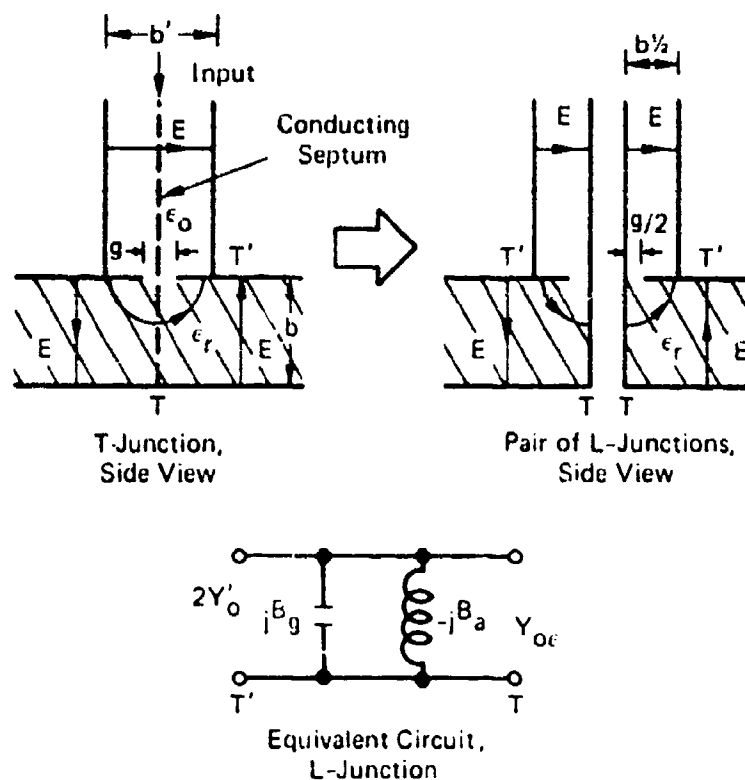
Fig. A-2 Bifurcated T-Junction

$$\frac{B_g}{Y_{o\epsilon}} = \frac{8b}{\lambda_{g\epsilon}} \left(\ln \frac{2\sqrt{2bb'}}{\pi g} - \frac{1}{2} \ln \left(\frac{2b'}{\pi g}\right) - \frac{1}{12} \left(\frac{\pi g}{2b'}\right)^2 \right.$$

$$+ \left(\frac{1}{\lambda_{g\epsilon}}\right)^2 \left\{ b^2 - \left(\frac{b'}{2}\right)^2 \left[1 - \frac{1}{2}\left(\frac{\pi g}{2b'}\right)^2\right]^4 \right\}$$

$$\left. + \left(\frac{\lambda_{g\epsilon}}{\lambda_g}\right)^2 \left\{ \frac{1}{2} \ln \left(\frac{2b'}{\pi g}\right) - \frac{1}{12}\left(\frac{\pi g}{2b'}\right)^2 - \frac{1}{4}\left(\frac{b'}{\lambda_g}\right)^2 \left[1 - \frac{1}{2}\left(\frac{\pi g}{2b'}\right)^2\right]^4 \right\} \right), b \ll \lambda_{g\epsilon}$$

$$(A-7b)$$

$$\frac{B_a}{Y_{o\epsilon}} = \frac{b}{\lambda_{g\epsilon}} \left(\frac{\pi g}{4b}\right)^2 , \quad g \ll b \qquad (A-8)$$

GRATING OF METALLIC POSTS

The equivalent circuit of the feed probes is arrived at by considering a planar grating of metallic posts and closely spaced resistors in free space as depicted in Fig. A-3. Axes of the posts are parallel to the electric field of an incident plane wave arriving at angle θ. The equivalent circuit for a grating of posts has been derived by Marcuvitz (Ref. 15, pp. 285-289) (as in the figure, but without the resistors). When the radiating medium is dielectric rather than free space, appropriate substitutions in the element values can be made, and the circuit values for the grating of posts may be written as

$$\frac{X_{a\epsilon}}{Z_{o\epsilon}} \approx \frac{a \cos \theta_\epsilon}{\lambda_\epsilon} \left[\ln\left(\frac{a}{2\pi r_o}\right) + 0.601 \left(3 - 2\cos^2\theta_\epsilon\right)\left(\frac{a}{\lambda_\epsilon}\right)^2 \right], \quad a/\lambda_\epsilon \ll 1$$

$$(A-9)$$

- 68 -
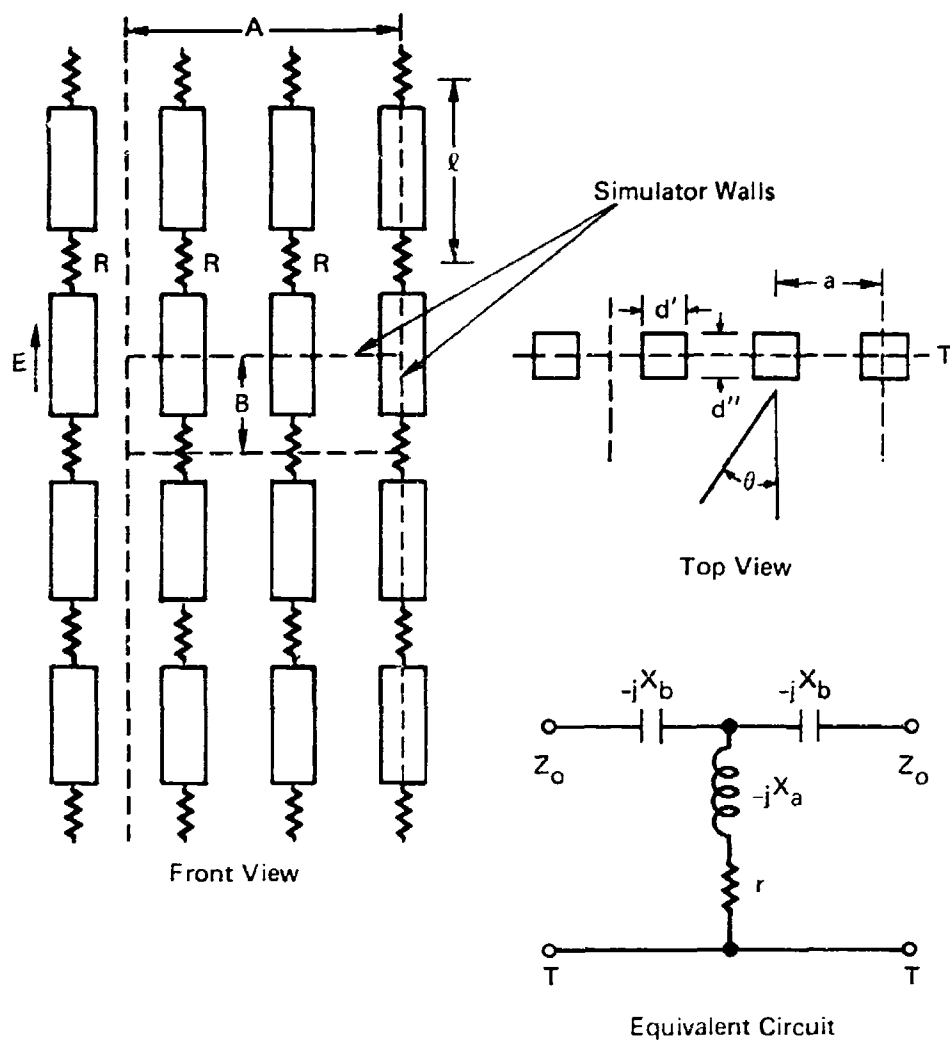
Fig. A-3 Grating of Posts with Series Resistors

$$\frac{X_{a\epsilon}}{Z_{o\epsilon}} \approx \frac{a \cos \theta_\epsilon}{\lambda_\epsilon} \left[\ln\left(\frac{a}{2\pi r_o}\right) + \left(14.5 - 13 \cos \theta_\epsilon\right)\left(a/\lambda_\epsilon\right)^3 \right] ,$$

$$a/\lambda \approx 0.5 \tag{A-10}$$

$$\frac{X_{b\epsilon}}{Z_{o\epsilon}} = \frac{a \cos \theta_\epsilon}{\lambda_\epsilon} \left(\frac{2\pi r_1}{a}\right)^2 \tag{A-11}$$

where

$2r_o = d$, $2r_1 = d$ for circular cross section — case a,

$2r_o = d'/2$, $r_1 = 0$ for coplanar ribbon posts — case b, and

$2r_o = d''/2$, $2r_1 = d''/2$ for ribbon posts perpendicular to grating plane — case c.

Equation (A-10) is obtained from fitting a curve to Marcuvitz's plots for the complete expression. The equivalent radii for cases b and c are for rectangular posts with one dimension set to zero.

If small resistors are placed close together and in series in each of the posts, the previous equivalent circuit is adapted to include a resistive component (Fig. A-3). The resistive component has the value $r = R \cdot a/\ell$ expressed in ohms per square, and can be understood by considering a square with sides D where $n\ell$ · ma - D. For convenience let D take any value such that n and m are integers. In the D by D square there are m columns of resistors where each column has n resistors in series, resulting in a total resistance for the square of $\frac{1}{m}$ (nR) ohms or $r = \frac{n}{m} R$ ohms per square. Since, from the above, $n\ell = ma$, it can be seen that $r = R\, a/\ell$ ohms per square.

A pair of vertical conducting walls may be inserted that are normal to and pass through the grating to form an

- 70 -

infinitely high waveguide. In the waveguide region plane
wave propagation is simulated at some incident angle. The
walls must pass either through the axis of the posts or
midway between the posts to maintain the simulation. Hori-
zontal top and bottom walls can be included in symmetry
planes, leaving the contained fields undisturbed. If the small
resistors are replaced by coaxial terminations at one hori-
zontal wall, then the simulated array of posts is identical
to the feed probes with the equivalent circuit shown and the
impedances of Eqs. (A-9), (A-10), and (A-11) where

$r = R \dfrac{B/\ell}{A/a}$ expressed in ohms for the A by B simulator

section. Here R is equal to twice the coaxial termination.

APERTURE EQUIVALENT CIRCUIT

A simulated array of strip radiators, shown earlier
in Fig. 3, has the equivalent circuit given in Fig. A-4 for
each half-unit cell. R_p is the coaxial termination of each
feed probe. The circuit is formed by combining the cir-
cuits of the L-junction and the feed probes. The slit-
coupled L-junction and feed probes are separated by a
length $(d_E - s)/2$ (characteristic impedance $Z_{0\epsilon}$) with a
short-circuited length of guide shunted across the probes.
Circuit values, normalized to guide impedances, are de-
rived as previously discussed.
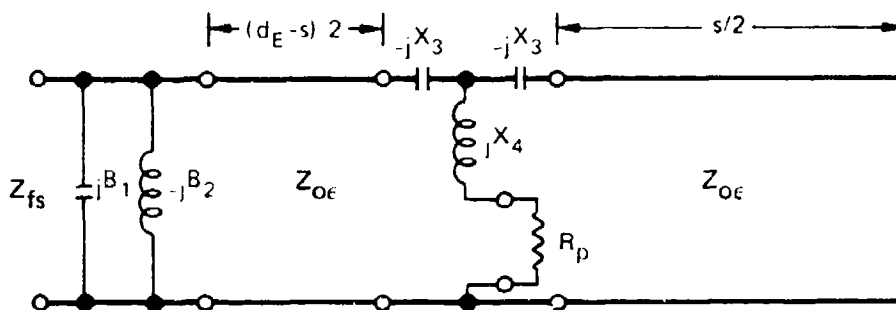
Fig. A-4 Equivalent Circuit, Array of Strip Radiators (H-plane scan)

The simulated strip radiator antenna model contains both waveguide components and coaxial elements (the exciting probe terminations). Absolute impedance concepts are ambiguous in waveguide, although not in coaxial, and a problem arises in assigning values to the normalizing impedances that appear in circuit expressions (Ref. 16). A somewhat arbitrary choice is to use plane waves in a waveguide simulator. Furthermore, it is convenient in this aperture model to consider antenna impedances on a half-unit cell basis so that one feed probe is included in each half-cell. Thus the normalizing impedances appearing in previous expressions are given by

$$Z_o' = \left(\frac{1}{2} d_E / d_H \right) \eta / \cos \theta_o, \text{ air-filled region} \quad (A-12)$$

$$Z_{o\epsilon} = b / d_H \eta / \left(\sqrt{\epsilon_r} \cos \theta_\epsilon \right), \text{ dielectric-filled region, and} \quad (A-13)$$

$$Z_o' = 1/Y_o',$$

$$Z_{o\epsilon} = 1/Y_{o\epsilon}.$$

The impedance of free space per half-unit cell is given by Eq. (A-12).

The incident arrival angle of plane waves in the simulator (the simulated scan angle) and the arrival angle of plane waves in the aperture dielectric region are, of course, different. The two angles are related by

$$\theta_o = \sin^{-1} \lambda / \lambda_c, \quad (A-14)$$

$$\theta_\epsilon = \sin^{-1} \lambda_\epsilon / \lambda_c. \quad (A-15)$$

Ref. 16.   C. C. Montgomery, R. H. Dicke, and E. M. Purcell, Principles of Microwave Circuits, Vol. 8, MIT Radiation Laboratory Series, New York: McGraw-Hill, 1948, pp. 66-67.

- 72 -

resulting in

$$\sin \theta_\epsilon = \frac{1}{\sqrt{\epsilon_r}} \sin \theta_o \, . \qquad \text{(A-16)}$$

where

$$\lambda_\epsilon = \lambda / \sqrt{\epsilon_r} \, .$$

Thus, the H-plane scanning model of an array of strip radiators, which is identical to that of the simulated aperture, has absolute circuit values referenced to a half-unit cell as written below. The previously derived circuit values have been denormalized using Eqs. (A-12) and (A-13), referenced to the H-plane scan angle through Eq. (A-16), and rewritten for convenience in the following equations in terms of strip width.

$$B_1 = \frac{8d_H}{\lambda} \cdot \frac{\epsilon_r - \sin^2 \theta_o}{x} \left(\left[\frac{1}{2} \ln \frac{2b}{\lambda} - \frac{1}{2} \ln \frac{d_E}{\lambda} - \frac{1}{2} \ln \frac{\pi}{2} \left(1 - \frac{w}{d_E} \right) - \frac{1}{12} \left(\frac{\pi}{2} \right)^2 \left(1 - \frac{w}{d_E} \right)^2 \right] \right.$$

$$+ \left(\epsilon_r - \sin^2 \theta_o \right) \left\{ \left(\frac{b}{\lambda} \right)^2 - \left(\frac{d_E}{2\lambda} \right)^2 \left[1 - \frac{1}{2} \left(\frac{\pi}{2} \right)^2 \left(1 - \frac{w}{d_E} \right)^2 \right]^4 \right\}$$

$$+ \frac{1 - \sin^2 \theta_o}{\epsilon_r - \sin^2 \theta_o} \left\{ -\frac{1}{2} \ln \frac{\pi}{2} \left(1 - \frac{w}{d_E} \right) + \frac{1}{12} \left(\frac{\pi}{2} \right)^2 \left(1 - \frac{w}{d_E} \right)^2 \right.$$

$$\left. \left. + \left(\frac{d_E}{2\lambda} \right)^2 \left(1 - \sin^2 \theta_o \right) \left[1 - \frac{1}{2} \left(\frac{\pi}{2} \right)^2 \left(1 - \frac{w}{d_E} \right)^2 \right]^4 \right\} \right) \qquad \text{(A-17)}$$

$$B_2 = \frac{d_H}{\lambda} \left(\frac{d_E}{\lambda} \right)^2 \left(\frac{\lambda}{b} \right)^2 \frac{\epsilon_r - \sin^2 \theta_o}{x} \left(\frac{\pi}{4} \right)^2 \left(1 - \frac{w}{d_E} \right)^2 \qquad \text{(A-18)}$$

$$X_3 = \frac{b}{\lambda} \varkappa \left(\frac{\pi d_1}{d_H}\right)^2 \tag{A-19}$$

$$X_4 = \frac{b}{\lambda} \varkappa \left[\ln \frac{d_H}{\pi d_o} + \left(14.5 - 13.0 \sqrt{1 - \frac{\sin^2 \theta_o}{\epsilon_r}}\right)\left(\sqrt{\epsilon_r} \, d_H/\lambda\right)^2 \right] \tag{A-20}$$

$$Z_{o\epsilon} = \frac{b}{d_H} \frac{\varkappa}{\sqrt{\epsilon_r - \sin^2 \theta_o}} \tag{A-21}$$

$$\beta_\epsilon = \left(\frac{2\pi}{\lambda}\right)\sqrt{\epsilon_r - \sin^2 \theta_o} \tag{A-22}$$

$$Z_{fs} = \frac{1}{2} \frac{d_E}{d_H} \frac{\varkappa}{\cos \theta_o} \tag{A-23}$$

where $d_o = d$, $d_1 = d$ for circular posts,

$d_o = d,' \rightarrow d_1 = 0$ for coplanar ribbon posts, and

$d_o = d'$, $d_1 = 2d''$ for ribbon posts perpendicular to grating plane.

EXPERIMENTAL VALIDATION

A computer program was written to calculate the aperture admittance for an array of strip radiators with circular probes. The array as constructed and analyzed had a 1.0-inch-thick aperture dielectric with $\epsilon_r = 2.5$. E- and H-plane spacings were 3.75 inches. The strip width was 3.5 inches, and excitation probes were separated by 2.75 inches. Probes in this aperture were No. 3-48 threaded brass rod sections, 7/64 inch in diameter,

screwed into tapped solder cups of type N connectors. The probe diameter was taken as 0.100 inch for the calculations.

Admittance measurements were performed in a waveguide simulator with E- and H-dimensions of 7.5 and 15.0 inches, respectively. Eight array elements were included in the simulation. Each element probe was terminated in 50 ohms. Predicted and measured admittance points over the frequency band of 0.5 to 1.0 GHz are shown on the Smith chart in Fig. A-5. Measured and predicted values are seen to be very close where the measured values are slightly more capacitive than calculated.

d_E=3.75 inches
d_H=3.75 inches
ϵ_r=2.5, b=1.0 inch
Strip Width=3.5 inches
Probe Separation=2.75 inches
Probe Diameter=0.100 inch

0.9 GHz-26°
1.0 GHz-23°
0.8 GHz-29°
Predicted
Measured
0.7 GHz-34°
0.5 GHz-52°
0.6 GHz-41°
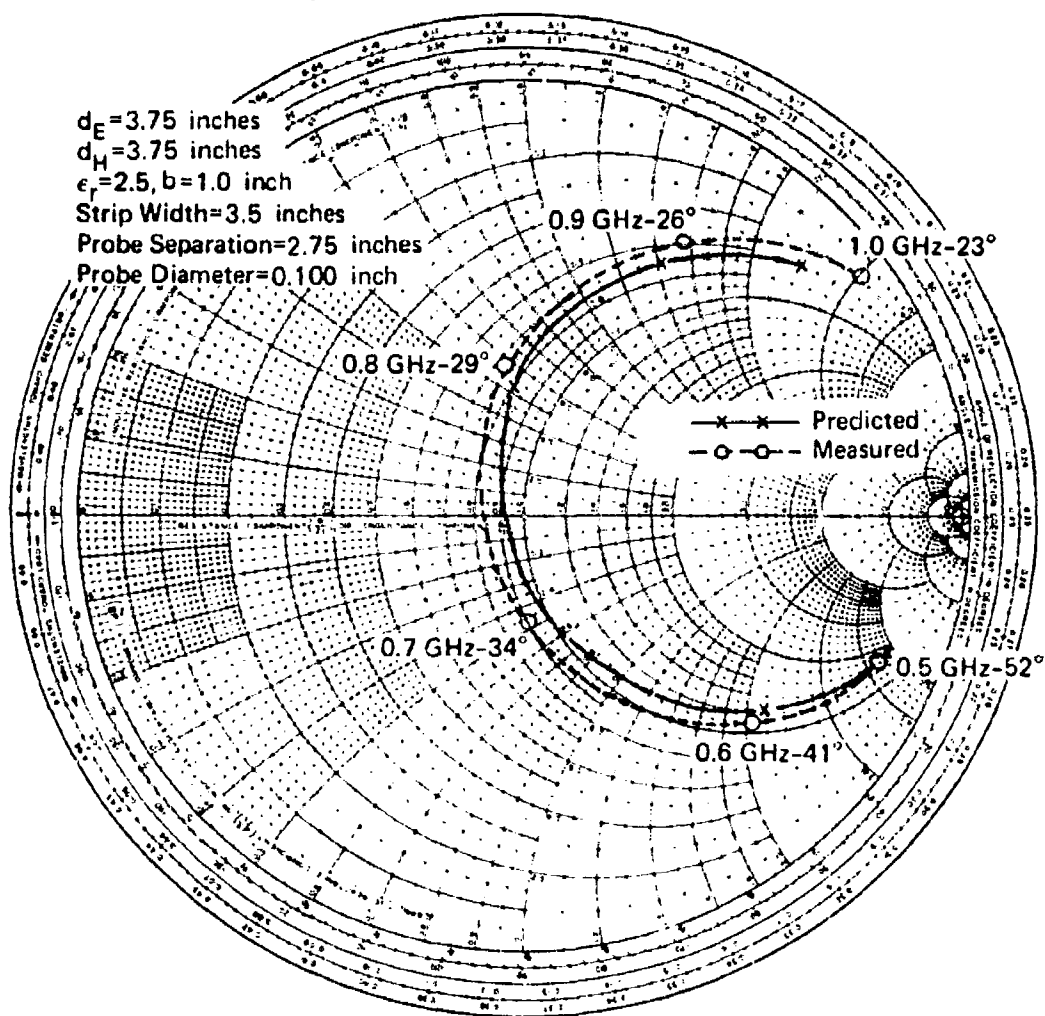
Fig. A-5 Aperture Admittance versus Frequency for Array of Strip Radiators

Appendix B

EFFECTS OF PROBE LOCATION ON ACTIVE ELEMENT IMPEDANCE OF ARRAY OF STRIP RADIATORS

The effects of moving the probes inward from the strip edges are found using the circuit of Fig. B-1a which represents one-half of the strip radiator immediately under the strip. Z_1 is that part of the active element impedance that is seen looking out from the strip edge. The length $l/2$ is the distance each probe is moved inward from the edges, and $s/2$ is the distance from strip center to probe. Transforming impedance Z_1 through $l/2$, paralleling the short-circuit stub, and adding in series the probe inductance, X_4, results in the broadside active element impedance per probe. For small values of $l/2$, the transforming line may be approximated by a series inductance. The short-circuit stub may be approximated by a stub of length $w/2$ with a negative series inductance (length $l/2$ removed), resulting in the circuit shown in Fig. B-1b. In Fig. B-1c the stub is replaced by its lumped equivalent. The active element impedance at each probe is given by

$$Z_e = - \frac{(X_1 + X)(X_2 - X) + j R_1 (X_2 - X)}{R_1 + j (X_1 + X_2)} + j X_4 , \quad \text{(B-1)}$$

from which the resistance is found to be

$$R_e = \frac{R_1 (X_2 - X)^2}{R_1^2 + (X_1 + X_2)^2} . \quad \text{(B-2)}$$

Letting R(s) equal the resistance when the probes are separated by s, and dividing by the resistance R(w) when the probes are at the strip edges results in

$$\frac{R(s)}{R(w)} = \left(1 - \frac{X}{X_2}\right)^2 . \quad \text{(B-3)}$$

- 77 -
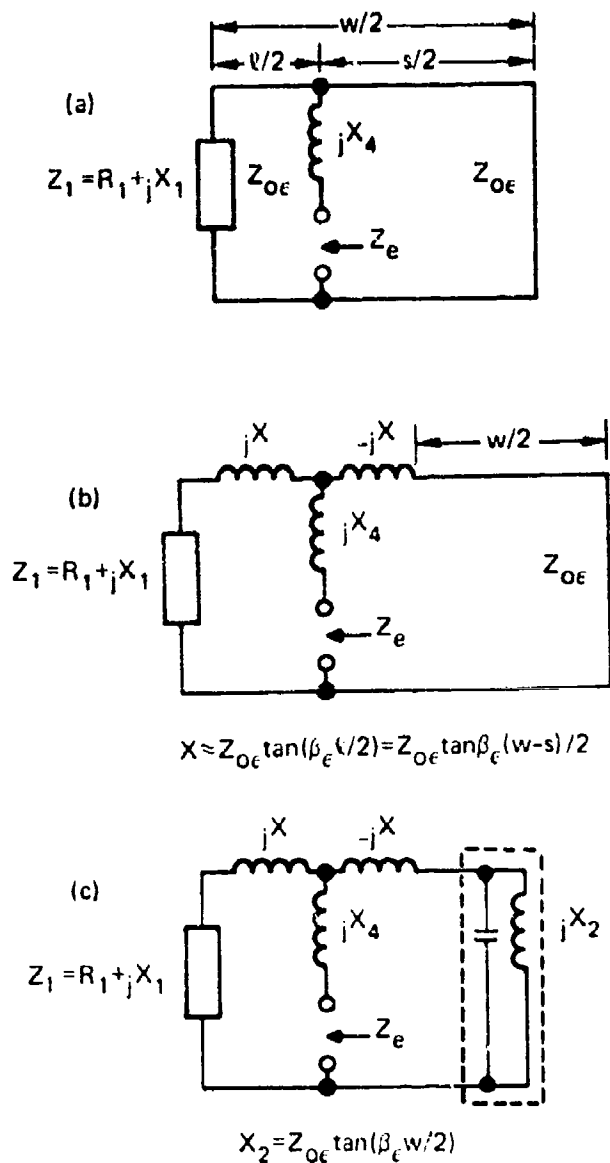
Fig. B-1 Circuit for Effects of Moving Probes Inward from Strip Edges

or

$$\frac{R(s)}{R(w)} = \frac{\tan(\beta_\epsilon\, \ell/2)}{\tan(\beta_\epsilon\, w/2)} \qquad . \qquad\qquad (B\text{-}4)$$

Approximating for small $\beta_\epsilon\, \ell/2$ and letting $\ell/2 = (w-s)/2$ results in

$$\frac{R(s)}{R(w)} \approx \left(1 - \frac{(1 - s/w)\,\beta_\epsilon\, w/2}{\tan(\beta_\epsilon\, w/2)}\right)^2 \qquad . \qquad\qquad (B\text{-}5)$$

Appendix C

COMPUTER PROGRAM LISTING (CPS LANGUAGE)
FOR STRIP RADIATOR ANALYSIS

The computer program listing for strip radiator
analysis, in Conversational Program System (CPS) lan-
guage, is given in the following pages.

```
100.        /* Glaupolin Strip Element Design */;
110.        DECLADE ans CHAR(3) VAR, ans? CHAR(5) VAR, s1 CHAR(1), s? CHAR(1), s? CHAR(1), s4 CHAR(1);
120.        pism_list;
130.        PUT LIST('Rectangular Spacing - Dimensions in inches');
140.        PUT LIST('Probes:   1    "    1    1");
150.        r=50/* 50 ohm loads */;
160.        PUT LIST('H-Plane Spacing');
170.        GET LIST(a);
180.        PUT LIST('E-Plane Spacing');
190.        GET LIST(b);
200.        h=b/2;
210.        PUT LIST('Strip Width');
220.        GET LIST(w);
230.        w=w/2;
240.        d=h-w;
250.        PUT LIST('Relative Dielectric Constant');
260.        GET LIST(er);
270.        PUT LIST('Dielectric Thickness');
280.        GET LIST(t);
290.        PUT LIST('Probe Separations');
300.        GET LIST(dp);
310.        dp=dp/2;
320.        PUT LIST('Probe Diameter or Width');
330.        GET LIST(c);
340.        PUT LIST('Is there a series capacitor- "yes" or "no"- use single quote around answer');
350.        GET LIST(ans);
360.        IF ans='yes' THEN PUT LIST('Series Capacitance in pfd');
370.        IF ans='yes' THEN GET LIST(ca);
380.        PUT LIST('Are simultance angles to be included-"yes" or "no"-use single quote around answer');
390.        GET LIST(ans2);
400.        IF ans2='yes' THEN PUT LIST('Simulated Width');
410.        IF ans2='yes' THEN GET LIST(ci);
420.        PUT LIST('Theta       normalized       "normalized";
430.        PUT LIST('        Transmit   v    usin   ,   Receive   v');
440.        PUT LIST('From');
450.        GET LIST(f);
460.        IF f<.001 THEN GO TO #100;
470.        a1=11.P/f;
480.        IF ans2='yes' THEN caneal/(cart(1-(a)/(*pC))*c*/a*c*C)/a*n of simulated angle */;
490.        IF ans2='yes' THEN phatanatand(ans)/simulated angle */;
500.        tmin=0;
510.        tmax=80;
520.        tt=tmin;
530.        DO theta=tmin to tmax by tstep;
540.        angle=theta/57.?;
550.        IF ans2='yes' THEN f((phase-atan(phase-std-std-tstan) THEN angle=phase/57.?;
560.        ;
570.        s1=sin(angle);
580.        co=cos(angle);
590.        t?=co;
600.        t1=cart(er-si*o?);
```

```
610.    bb=4*t1**2/a1*(log(2*sqrt(t*h)/(p1+d))+(t*t/a1**2);
620.    c1=log(2*b/(p1+d))*(p1+d)/(2*h))**2/6;
630.    c2=(1-.5*(p1+d)/(2*h))**4);
640.    ber=2*(1**2/a1*(c1+2*(h*t/a1)**2*.2);
650.    hec=2*t*2/a1*(c1+2*(b*t2/a1)**2*c2);
660.    bt=a/377*(2*bh-.5*ber*.5+an);
670.    ba=-a/377*(n1*d/(2*t1)+2*t1*t2/a1);
680.    xb=-t*377/a1*(p1+s/(1.h1h*a1)**2;
690.    xc=t*377/a1*(log(a/(p1+c/2))+(16.5-t*t1/sqrt(er))*(a/a1)**x);
700.    IF ans=.yes% THEU xc=xc-10*t*/(2*p1e*can);
710.    bs=-a/(t*377)*t1*cos(2*p1+dn*t1/a1);
720.    bs=bs/sin(2*p1+dn*t1/a1);
730.    /* Element Values Calculated */;
740.    /* Begin Receive Impedance */;
750.    x1=xb-1/bs;
760.    g1=r/(r**2+xc**2);
770.    b1=-xc/(r**2+xc**2)-1/x1;
...     r1=r1/(g1**2+b1**2);
800.    x1=-b1/(g1**2+b1**2)+xh;
810.    beta=2*p1*t1/a1;
820.    zo=t*377/(a*t1);
830.    tan=sin(beta*(h-dn))/cos(beta*(h-dn));
840.    r1=r1/zo;
850.    x1=x1/zo;
860.    ix=2;
870.    CALL comp2(ix,r1,x1+tan,1-x1*tan,r1*tan,r ,x1);
880.    r1=r1*zo;
890.    x1=x1*zo;
900.    g1=r1/(r1**2+x1**2);
930.    b1=-x1/(r1**2+x1**2)+ba+bt;
940.    vfs=a*co/(b*377);
950.    rfs=g1/vfs;
960.    bfs=b1/vfs;
970.    rfs=rfs/(rfs**2+bfs**2);
980.    xfs=-bfs/(rfs**2+bfs**2);
990.    /* End of Receive */;
1000.   /* Begin Transmit */;
1010.   g1=vfs;
1020.   b1=ht+ba;
1030.   r1=g1/(g1**2+b1**2)/zo;
1040.   x1=-(b1/(g1**2+b1**2))/zo;
1050.   CALL comp2(ix,r1,x1+tan,1-x1*tan,r1*tan,r1,x1);
1060.   r1=r1*zo;
1070.   x1=x1*zo+xh;
1080.   g1=r1/(r1**2+x1**2);
1090.   b1=-x1/(r1**2+x1**2)-1/(xh-1/hs);
1100.   rxm=r1/(g1**2+b1**2)/r;
        xxm=-b1/(g1**2+b1**2)+xc)/r;
        pxm=rxm/(rxm**2+xxm**2);
        bxm=-xxm/(rxm**2+xxm**2);
```

- 82 -

```
1110.          /* End of Transmit */;
1120.          rho=sqrt(((rfs-1)**2+xfs**2)/((rfs+1)**2+xfs**2));
1130.          vswr=(1+rho)/(1-rho);
1140.          s1,s2,s3,s4='+';
1150.          IF xxm<0 THEN s1=1-1;
1160.          IF hxm<0 THEN s2=1-1;
1170.          IF xfs<0 THEN s3=1-1;
1180.          IF bfs<0 THEN s4=1-1;
1190.          PUT IMAGE(angle=57.3,rxm,s1,abs(xxm),pxm,s2,abs(hxm),vswr,rfs,s3,abs(xfs),pfs,s4,abs(bfs))(11);
1200.          IMAGE;
----. ------------------------------------------------------------------------
11:            IF ans2=1 yes!angle=theta/57.3 THEN angle=theta/57.3; ELSE GO TO #7;
1210.          GO TO #2;
1230.    #7:   END #7;
1240.          GO TO #t;
1250.    comp2: PROCEDURE (ind,cna,cnb,cnc,cnd,cne,cnf);
1260.          /* ind=1 - mult, ind=2 - div */;
1270.          IF ind=2 THEN GO TO div;
1280.          cne=cna*cnc-cnb*cnd;
1290.          cpf=cna*cnd+cnb*cnc;
1300.          RETURN;
1310.    div:  cne=(cna*cnc+cnb*cnd)/(cnc**2+cnd**2);
1320.          cpf=(-cna*cnd+cnb*cnc)/(cnc**2+cnd**2);
1330.          RETURN;
1340.          END comp2;
```

- 83 -

Appendix D

COMPUTER PRINT OUT - ARRAY OF STRIP RADIATORS
UNDER H-PLANE SCAN CONDITIONS

```
Rectangular Spacing - Dimensions in inches
Probes: |  |  |  |  |
H-Plane Spacing=
a
3.75
E-Plane Spacing=
b
3.75
Strip Width=
w
3.1
Relative Dielectric Constant=
er
2.5
Dielectric Thickness=
t
1.5
Probe Separation=
dp
2.75
Probe Diameter or Width=
s
.200
is there a series capacitor- "yes" or "no"- use single quote around answer
ans
'yes'
Series Capacitance in pf=
cap
2.2
Are simulator angles to be included-"yes" or "no"-use single quote around answer
ans2
'yes'
Simulator Width=
SW
15.0
```

Theta Deg	Z	Normalized Transmit	Y	VSWR	Z	Normalized Receive	Y
Freq=							
f							
.5							
0.	1.45 -j	0.32	0.66 +j 0.15	1.58	1.11 -i	0.47	0.76 +i 0.32
10.	1.42 -j	0.29	0.68 +j 0.14	1.53	1.13 -i	0.43	0.77 +i 0.30
20.	1.30 -j	0.21	0.75 +j 0.12	1.39	1.16 -i	0.31	0.91 +i 0.22
30.	1.12 -j	0.12	0.88 +j 0.10	1.19	1.14 -i	0.10	0.87 +i 0.08
40.	0.89 -j	0.06	1.11 +i 0.08	1.14	1.01 +i	0.13	0.98 -i 0.13
50.	0.66 -j	0.05	1.50 +j 0.11	1.52	0.76 +i	0.28	1.16 -i 0.43
52.	0.62 -j	0.05	1.60 +j 0.13	1.62	0.71 +i	0.29	1.20 -i 0.50
60.	0.45 -j	0.07	2.16 +j 0.33	2.22	0.50 +i	0.30	1.48 -i 0.98

Freq=
f
.6

0.	2.35 -j	0.72	0.39 +j	0.12	2.62	0.41 -i	0.26	1.72 +i 1.10
10.	2.39 -j	0.64	0.39 +i	0.10	2.50	0.42 -i	0.26	1.74 +i 1.07
20.	2.47 -j	0.37	0.40 +j	0.06	2.53	0.42 -i	0.23	1.82 +i 1.01
30.	2.48 +j	0.10	0.40 -i	0.02	2.48	0.42 -i	0.19	1.96 +i 0.90
40.	2.26 +j	0.69	0.41 -i	0.12	2.51	0.41 -i	0.14	2.10 +i 0.76
41.	2.22 +j	0.74	0.41 -i	0.14	2.52	0.41 -i	0.14	2.22 +i 0.74
50.	1.77 +j	1.16	0.40 -i	0.26	2.73	0.37 -i	0.08	2.58 +i 0.57
60.	1.19 +j	1.38	0.36 -i	0.42	3.33	0.30 -i	0.03	3.29 +i 0.33

Freq=
f
.7

0.	1.63 -j	1.13	0.41 +j	0.29	2.55	0.39 -i	0.09	2.49 +i 0.60
10.	1.70 -j	1.13	0.41 +i	0.27	2.57	0.38 -i	0.09	2.52 +i 0.57
20.	1.93 -j	1.11	0.39 +j	0.22	2.71	0.37 -i	0.07	2.62 +i 0.46
30.	2.37 -j	0.98	0.36 +j	0.15	2.84	0.35 -i	0.04	2.81 +i 0.30
34.	2.62 -j	0.85	0.35 +j	0.11	2.94	0.34 -i	0.02	2.92 +i 0.19
40.	3.02 -j	0.54	0.32 +j	0.06	3.13	0.32 -i	0.00	3.13 +i 0.03
50.	3.62 +j	0.56	0.27 -j	0.04	3.71	0.27 +i	0.02	3.68 -i 0.34
60.	3.36 +j	2.16	0.21 -j	0.14	4.94	0.21 +i	0.04	4.66 -i 0.08

Freq=
f
.8

0.	0.95 -j	0.64	0.72 +j	0.49	1.92	0.52 -i	0.04	1.90 +i 0.13
10.	0.99 -j	0.67	0.69 +i	0.47	1.93	0.52 -i	0.02	1.92 +i 0.09
20.	1.12 -i	0.74	0.62 +i	0.41	2.00	0.50 +i	0.01	2.00 -i 0.04
29.	1.36 -j	0.85	0.53 +i	0.33	2.15	0.46 +i	0.06	2.12 -i 0.26
30.	1.38 -j	0.86	0.52 +i	0.32	2.15	0.46 +i	0.06	2.13 -i 0.27
40.	1.88 -j	1.01	0.41 +i	0.22	2.56	0.40 +i	0.11	2.35 -i 0.53
50.	2.82 -j	1.00	0.31 +i	0.12	3.29	0.31 +i	0.13	2.75 -i 1.15
60.	4.56 -j	0.59	0.22 +j	0.03	4.54	0.22 +i	0.12	3.47 -i 1.95

Freq=
f
.9

0.	0.62 -j	0.02	1.62 +j	0.04	1.62	0.71 -i	0.28	1.22 +i 0.40
10.	0.64 -j	0.04	1.56 +i	0.09	1.57	0.72 -i	0.26	1.23 +i 0.45
20.	0.71 -j	0.11	1.38 +i	0.21	1.45	0.74 -i	0.18	1.27 +i 0.32
26.	0.78 -j	0.18	1.22 +i	0.28	1.38	0.74 -i	0.11	1.31 +i 0.20
30.	0.84 -j	0.24	1.10 +j	0.31	1.36	0.74 -i	0.05	1.35 +i 0.09
40.	1.09 -j	0.46	0.78 +j	0.33	1.56	0.66 +i	0.11	1.49 -i 0.24
50.	1.53 -j	0.81	0.51 +i	0.27	2.15	0.49 +i	0.21	1.72 -i 0.73
60.	2.39 -j	1.39	0.31 +j	0.18	3.31	0.32 +i	0.22	2.15 -i 1.47

Freq=
f
1.0

0.	0.45 +i	0.58	0.84 -i	1.09	3.12	0.45 -i	0.58	0.83 +j 1.09
10.	0.46 +j	0.56	0.88 -i	1.07	2.99	0.47 -i	0.58	0.84 +i 1.04
20.	0.50 +i	0.50	1.00 -i	1.00	2.52	0.54 -i	0.58	0.86 +i 0.92
23.	0.52 +j	0.47	1.06 -i	0.96	2.47	0.58 -i	0.57	0.87 +i 0.87
30.	0.58 +j	0.39	1.19 -i	0.81	2.10	0.68 -i	0.54	0.91 +i 0.72
40.	0.71 +j	0.21	1.30 -j	0.38	1.52	0.85 -i	0.36	0.99 +i 0.42
50.	0.92 -j	0.10	1.07 +j	0.11	1.14	0.88 -i	0.01	1.14 +i 0.01
60.	1.27 -j	0.61	0.64 +j	0.31	1.79	0.61 +i	0.25	1.41 -i 0.57

Appendix E

SATURATED OUTPUT POWER AND EFFICIENCY OF RF TRANSISTORS OPERATING IN CLASS C

In this appendix we consider the transistor amplifier in Fig. E-1 where the transistor is assumed to have the idealized collector characteristics shown. Operation is in class B at the threshold of saturation, and the load is such that all frequencies other than the fundamental are optimally terminated in a short circuit (Ref. 17). Although class B operation s considered in this idealized circuit, a practical transistor would be just over the threshold into class C operation. The expressions developed here are assumed to be approximately valid for practical circuits.

For the idealized circuit the collector current under class B operation is given by

$$
\left.
\begin{aligned}
i_c &= I \sin \omega_0 t, \quad 2n\pi < \omega_0 t < (2n+1)\pi \\
&= 0, \quad (2n+1)\pi < \omega_0 t < (2n+2)\pi
\end{aligned}
\right\}, \quad n = 0,1,2,\ldots \tag{E-1}
$$

A Fourier series expansion results in

$$
i_c = I\left(\frac{1}{\pi} + \frac{1}{2}\sin \omega_0 t - \frac{2}{\pi}\sum \frac{1}{n^2-1}\cos n\,\omega_0 t\right), \quad n = 2,4,6,\ldots
$$

$$\tag{E-2}$$

At the threshold of saturated class B operation the collector voltage swings to a minimum level of v_{sat}. Since all harmonic components of the voltage are terminated by a short circuit, the collector voltage has only DC and fundamental frequency components, as given by

Ref. 17.   D. M. Snider, "A Theoretical Analysis and Experimental Confirmation of the Optimally Load'd and Overdriven RF Power Amplifier," IEEE Transactions on Electron Devices, Vol. ED-14, December 1967, pp. 851-857.
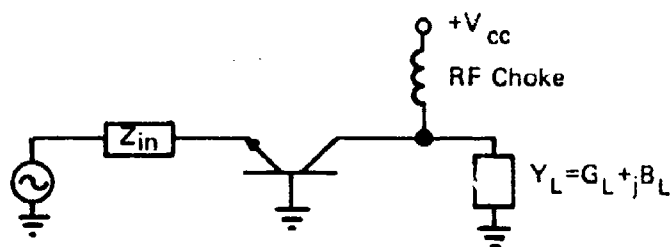
(a) Grounded Base RF Amplifier
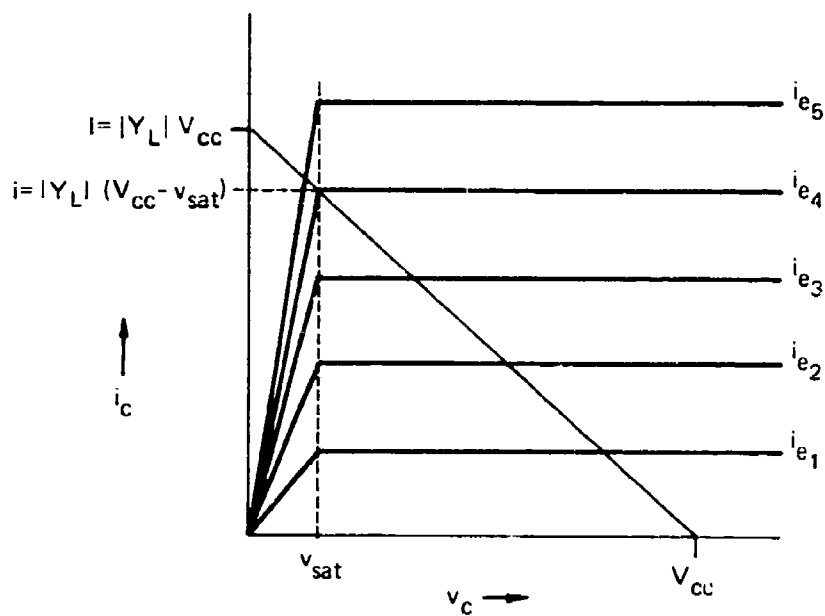
(b) Transistor Collector Characteristics
(grounded base)

Fig. E-1 Schematic of RF Amplifier and Transistor Collector Characteristics

$$v_c = V_{cc} + (V_{cc} - v_{sat}) \sin(\omega_o t + \varphi). \qquad \text{(E-3)}$$

The relation between the fundamental components of collector current $(I/2)$ and collector voltage is given by

$$I/2 = (V_{cc} - v_{sat}) |Y_L| \qquad \text{(E-4)}$$

where

$$Y_L = G_L + jB_L \text{ at the fundamental frequency.}$$

Transistor saturated output power is found from the collector voltage across the real part of the load (DC blocked):

$$P_{RF} = 1/2 (V_{cc} - v_{sat})^2 G_L \qquad \text{(E-5)}$$

The DC power supplied by the power supply is the product of supply voltage and DC current:

$$P_{DC} = \frac{1}{\pi} I V_{cc} \qquad \text{(E-6)}$$

Substituting from Eq. (E-4) yields

$$P_{DC} = \frac{2}{\pi} V_{cc}(V_{cc} - v_{sat}) |Y_L| \qquad \text{(E-7)}$$

The collector efficiency in a transistor amplifier is given by

$$\varkappa_c = P_{RF}/P_{DC}. \qquad \text{(E-8)}$$

Substituting from Eqs. (E-5) and (E-6) results in

$$\varkappa_c = \frac{\pi}{4} \frac{V_{cc} - v_{sat}}{V_{cc}} |G_L/Y_L|. \qquad \text{(E-9)}$$

or

$$x_c = \frac{\pi}{4} \frac{V_{cc} - v_{sat}}{V_{cc}} \bigg/ \sqrt{1 + (B_L/G_L)^2} \; . \qquad (E\text{-}10)$$

NOMENCLATURE

A = waveguide simulator width

A_{eff} = effective antenna aperture area

a = spacing between gratings

b = dielectric thickness, dielectric-filled guide height

b' = height of coupled guide

B = waveguide simulator height

B_1 = capacitive susceptance in aperture equivalent circuit

B_2 = inductive susceptance in aperture equivalent circuit

B_a = inductive susceptance, partially filled L-junction

B_a' = inductive susceptance, partially filled T-junction

$B_{a\epsilon}$ = inductive susceptance, dielectric-filled T-junction

B_b' = capacitive susceptance, partially filled T-junction

$B_{b\epsilon}$ = capacitive susceptance, dielectric-filled T-junction

B_c = susceptance of symmetrical iris in air-filled guide

$B_{c\epsilon}$ = susceptance of symmetrical iris in dielectric-filled guide

B_g = capacitive susceptance, partially filled L-junction

B_L = transistor amplifier load susceptance

- 91 -

Preceding page blank

$B(\theta)$	=	dielectric sheet susceptance
β_ϵ	=	phase constant in dielectric
d	=	circular probe diameter
d'	=	rectangular probe width
d''	=	rectangular probe thickness
d_E	=	E-plane spacing
d_H	=	H-plane spacing
E	=	electric field
ϵ_o	=	free-space permittivity
ϵ_r	=	relative dielectric constant
η_c	=	collector efficiency
θ	=	plane wave incident angle relative to longitudinal direction
θ_c	=	electrical length for balun cavity center to end
θ_ϵ	=	plane wave incident angle relative to longitudinal direction in dielectric
θ_o	=	simulated scan angle
θ_s	=	electrical length of balun compensating line
φ	=	phase between collector current and voltage
G_L	=	transistor amplifier load conductance
g	=	coupling slit width
h	=	substrate thickness
I	=	peak collector current
i_c	=	instantaneous collector current
i_e	=	emitter current
n	=	120π, intrinsic impedance of free space
λ	=	free-space wavelength
λ_c	=	waveguide cut-off wavelength

λ_ϵ	=	wavelength in dielectric
λ_g	=	waveguide wavelength in air-filled guide
$\lambda_{g\epsilon}$	=	waveguide wavelength in dielectric-filled guide
P_{DC}	=	DC power
P_{RF}	=	RF output power
R	=	grating resistors
R_1	=	resistive part of Z_1
R_e	=	resistive part of active element impedance
R_p	=	coaxial termination
r	=	equivalent circuit resistance
R(s)	=	resistive part of active element impedance at probe separation, s
R(w)	=	resistive part of active element impedance at probe separation, w (strip edge)
s	=	probe separation
t	=	time
T, T'		reference planes
v_c	=	instantaneous collector voltage
V_{cc}	=	supply voltage
v_{sat}	=	saturation voltage
VSWR	=	voltage standing wave ratio
w	=	strip width
X	=	series reactance due to transformation length
$X_{a\epsilon}$		grating inductive reactance in dielectric medium
X_1		reactance of Z_1
X_2	=	reactance of short circuit stub w/2 in length
X_3	=	probe capacitive reactance

X_4 = probe inductive reactance

X_a = grating inductive reactance in free space

X_b = grating capacitive reactance in free space

$X_{b\epsilon}$ = grating capacitive reactance in dielectric medium

Y_L = transistor amplifier load admittance

Y_o' = characteristic admittance, air-filled guide of height b'

$Y_{o\epsilon}$ = characteristic admittance, dielectric-filled guide of height b

$Y_{o\epsilon}'$ = characteristic admittance, guide of height b'

Z_1 = aperture impedance looking out from strip edge

Z_c = balun cavity characteristic impedance

Z_e = active element impedance at each probe

Z_{fs} = free space impedance per unit half-cell at scanned angle

Z_{in} = balun input impedance

Z_L = impedance of each balun output line

Z_o' = characteristic impedance, air-filled guide

$Z_{o\epsilon}$ = characteristic impedance in dielectric-filled region

Z_s = impedance of balun compensating stub

ω = frequency, rad/s

REFERENCES

1. J. L. Allen, "On Array Element Impedance Varia-
    tion With Spacing," IEEE Transactions on Antennas
    and Propagation, Vol. AP-12, May 1964, pp. 371-
    372.

2. E. V. Byron, "A New Flush Mounted Antenna Ele-
    ment for Phased Array Application," Proceedings
    of the Phased-Array Antenna Symposium, 1970,
    pp. 187-192.

3. E. V. Byron, Antenna Aperture Design for Project
    Camel, APL/JHU TG 1101, February 1970.

4. G. J. Laughlin, E. V. Byron, and T. C. Cheston,
    "Very Wideband Phased-Array Antenna," IEEE
    Transactions on Antennas and Propagation, Vol.
    AP-20, November 1972, pp. 699-704.

5. P. W. Hannan and M. A. Balfour, "Simulation of a
    Phased-Array Antenna in Waveguide," IEEE Trans-
    actions on Antennas and Propagation, Vol. AP-13,
    May 1965, pp. 342-353.

6. N. Marchand, "Transmission-Line Conversion,"
    Electronics, Vol. 17, December 1944, pp. 142-
    145.

7. W. K. Roberts, "A New Wideband Balun," Proceed-
    ings of the IRE, December 1957, pp. 1628-1632.

8. J. W. McLaughlin, D. A. Dunn, and R. W. Grow,
    "A Wideband Balun," IRE Transactions on Micro-
    wave Theory and Techniques, Vol. MTT-6, July
    1958, pp. 314-316.

9. R. Bawer and J. J. Wolfe, "A Printed Circuit Balun for Use With Spiral Antennas," IRE Transactions on Microwave Theory and Techniques, Vol. MTT-8, May 1960, pp. 319-325.

10. G. Oltman, "The Compensated Balun," IEEE Transactions of Microwave Theory and Techniques, Vol. MTT-14, March 1966, pp. 112-119.

11. H. R. Phelan, "A Wideband Parallel-Connected Balun," IEEE Transactions of Microwave Theory and Techniques, Vol. MTT-18, May 1970, pp. 259-263.

12. G. J. Laughlin, Patent 3,827,001, July 1974.

13. E. G. Magill and H. A. Wheeler, "Wide-Angle Impedance Matching of a Phased Array Antenna by a Dielectric Sheet," IEEE Transactions on Antennas and Propagation, Vol. AP-14, January 1966, pp. 49-53.

14. W. H. Leighton, R. J. Chaffin, and J. G. Webb, "RF Amplifier Design With Large Signal S-Parameters," IEEE Transactions on Microwave Theory and Techniques, Vol. MTT-21, December 1973, pp. 809-814.

15. N. Marcuvitz, Waveguide Handbook, Vol. 10, MIT Radiation Laboratory Series, New York: McGraw-Hill, 1951.

16. C. G. Montgomery, R. H. Dicke, and E. M. Purcell, Principles of Microwave Circuits, Vol. 8, MIT Radiation Laboratory Series, New York: McGraw-Hill, 1948, pp. 66-67.

17. D. M. Snider, "A Theoretical Analysis and Experimental Confirmation of the Optimally Loaded and Overdriven RF Power Amplifier," IEEE Transactions on Electron Devices, Vol. ED-14, December 1967, pp. 851-857.

INITIAL DISTRIBUTION EXTERNAL TO THE APPLIED PHYSICS LABORATORY*

ORGANIZATION	LOCATION	ATTENTION	No. of Copies
DEPARTMENT OF DEFENSE			
DDC	Alexandria, Va.		12
Department of the Navy			
NAVSEA	Washington, D. C.	SEA-0341 (S. A. Barham, T. Tasaka)	2
		SEA-652B (R. T. Hill)	1
		SEA-09G3	2
NRL	Washington, D. C.	L. Whicker	1
NELC	San Diego, Cal.	J. H. Provencher	1
NSEC	Washington, D. C.	R. D. Lending	1
NAVAIR	Washington, D. C.	AIR-50174	2
NAVPRO	Silver Spring, Md.		1
CONTRACTORS			
MIT Lincoln Laboratory	Lexington, Mass.	C. Blake	1
Hughes Aircraft Co.	Fullerton, Cal.	J. Ajioka	1
RCA Missile & Surface Radar Division	Moorestown, N. J.	W. Patton	1
Raytheon	Santa Barbara, Cal.	D. Archer	1
Sperry Gyroscope Division	Great Neck, N. Y.	L. Schwartzman	1

*Initial distribution of this document within the Applied Physics Laboratory has been made in accordance with a list on file in the APL Technical Publications Group.

Notices of availability of this report have been sent to the following addressees, who comprise the distribution list for Quarterly Report Research and Development Programs at The Johns Hopkins University Applied Physics Laboratory, January-March 1975, APL/JHU C-RQR/75-1. They are not sent to offices listed in the initial distribution.

ORGANIZATION	LOCATION	ATTENTION
DEPARTMENT OF DEFENSE		
DDR&E	Washington, D.C.	Capt. R. C. Avrit
Dir., WSEG	Arlington, Va.	
Tactical Technology Info. Analysis Ctr.	Columbus, Ohio	Nancy Hall
DDC	Alexandria, Va.	
Information Analysis Ctr., CPIA	Silver Spring, Md.	
Defense Mapping Agency, Aerospace		PRA
Ctr.	St. Louis, Mo.	RDG
Department of the Navy		
Department Offices		
CNO	Washington, D.C.	OP-60
NAVSEASYSCOM	Washington, D.C.	SEA-00
		SEA-03
		SEA-03C (J. Huth)
		SEA-032

ORGANIZATION	LOCATION	ATTENTION
Department of the Army (cont'd)		
Centers		
Redstone Scientific Info. Ctr.	Huntsville, Ala.	Chief, Doc. Section
Laboratories		
Army Ballistic Research Labs.	Aberdeen Proving Ground, Md.	AMXBR-XM-SE
Arsenals		
Hq., Picatinny Arsenal	Dover, N.J.	STINFO
U.S. GOVERNMENT AGENCIES		
Security Agencies		
Central Intelligence Agency	Washington, D.C.	CSR/ADD/Std. Dist.
National Security Agency	Ft. Meade, Md.	C3/TDL
National Aero. and Space Admin.		
Headquarters	Washington, D.C.	RAP: N. Rekos (Code RLC)
Hq., Office of Space Sciences	Washington, D.C.	M. J. Aucremanne (Code SG)
Langley Res. Ctr.	Hampton, Va.	K. F. Rubert
		J. Henry
Lewis Res. Ctr.	Cleveland, Ohio	E. Lezberg
Flight Res. Ctr.	Edwards AFB, Cal.	J. Nugent (Prop.)
Ames Res. Ctr.	Moffett Field, Cal.	F. Pfyle 228.7
NASA Scientific and Technical Information Facility	College Park, Md.	J. Waldo
Goddard Space Flight Ctr.	Greenbelt, Md.	Library - 252
CONTRACTORS		
Automation Industries/Vitro Labs. Div.	Silver Spring, Md.	Report Acquis. ISA-14

ORGANIZATION	LOCATION	ATTENTION
Department of the Navy (cont'd)		
NAVSEASYSCOM (cont'd)	Washington, D.C.	SEA-032A
		SEA-033
		SEA-0331A
		SEA-034
		SEA-034B
		SEA-0462
		SEA-06G
		SEA-09G3
		SEA-55B
		SEA-6512
		SEA-653
		SEA-654
		SEA-6541
		SEA-6542
		SEA-6543
		SEA-65431
		SEA-65432
		PMS 304-20
		PMS 403-40
		PMS-404
		PMS 404-032
		PMS-405
CNM	Washington, D.C.	NMAT-03
		NMAT-031.
		NMAT-031.1 (Capt. Keach)
		NMAT-032
NAVAIRSYSCOM	Washington, D.C.	AIR-00
		AIR-03
		AIR-03B
		AIR-03C
		AIR-330
		AIR-5108
		AIR-520A
		AIR-520C
		AIR-5203
		AIR-535
		AIR-50174
Strategic Systems Project Office	Washington, D.C.	SSP-20
		SSP-24
		SSP-27
		SSP-272
NAVELEXSYSCOM, Navy Space Projects Office	Washington, D.C.	PME 106
NAVPRO	Silver Spring, Md.	
Office of Naval Research	Washington, D.C.	463
Laboratories		
Naval Surface Weapons Ctr.	White Oak, Md.	Library
		NOL-034
	Dahlgren, Va.	MIL
		DR:Colby
NRL	Washington, D.C.	2027
		6500 (W. R. Sooy)
		6506 (H. Gandy)

ORGANIZATION	LOCATION	ATTENTION
Department of the Navy (cont'd)		
Facilities		
NEODF	Indian Head, Md.	
Naval Ordnance Station	Indian Head, Md.	Tech. Library
NSWSES	Port Hueneme, Cal.	Tech. Library, Code 5100
		Eng. Directorate,
		Code 4000
		Talos Dept., Code 4200
Schools		
U.S. Naval Academy	Annapolis, Md.	Weapons Dept.
Naval Postgraduate School	Monterey, Cal.	Library, Tech. Rpts. Sec.
Naval Guided Missile School	Dam Neck, Va.	Library
Pac. Flt. Missile Weap. Sys. Tng. Unit	San Diego, Cal.	Library
Mare Is. Nav. Schools Command	Vallejo, Cal.	Guided Missile School
Centers		
Naval Intelligence Support Ctr.	Washington, D.C.	
NSRDC	Washington, D.C.	Aerodyn. Lab. Libr.
NWC	China Lake, Cal.	406
		45
		Tech. Library, 753
NELC	San Diego, Cal.	Tech. Library
NOSC, Naval Ammo. Depot	Crane, Ind.	NAPEC
Department of the Air Force		
Department Offices		
Hq. USAF	Washington, D.C.	AFRDD
Laboratories		
Aero. Propulsion Lab.	WPAFB, Ohio	F. D. Stull
Avionics Lab.	WPAFB, Ohio	AVO-2
Rocket & Propulsion Lab.	Edwards AFB, Cal.	RPMMM
		MKCO
Centers		
Arnold Eng'g Devel. Ctr. (AFSC)	Arnold AFS, Tenn.	DSC/Research, AER
Hq., AF Special Communications Ctr.	San Antonio, Texas	TDT
Commands		
Air Force Systems Command	Andrews AFB, Md.	SCTSP
		Tech. Libr./DPSL
Air University	Maxwell AFB, Ala.	Tech. Library
Department of the Army		
Commands		
Missile Command	Redstone Arsenal, Ala.	AMCPM-MDEM